Advanced Drug Delivery Reviews 138 (2019) 18–40

Contents lists available at ScienceDirect

Advanced Drug Delivery Reviews

journal homepage: www.elsevier.com/locate/addr

External stimulus responsive inorganic nanomaterials for cancer theranostics

Sheikh Mohamed M. [a,b], Srivani Veeranarayanan [a], Toru Maekawa [a,b,*], Sakthi Kumar D. [a,b,*]

[a] Bio-Nano Electronics Research Centre, Toyo University, Kawagoe, 350-8585, Japan
[b] Graduate School of Interdisciplinary New Science, Toyo University, Kawagoe 350-8585, Japan

ARTICLE INFO

Article history:
Received 2 July 2018
Received in revised form 3 September 2018
Accepted 8 October 2018
Available online 12 October 2018

Keywords:
Theranostics
Inorganic nanoparticles
External stimulus
Clinical trials
Cancer

ABSTRACT

Cancer is a highly intelligent system of cells, that works together with the body to thrive and subsequently overwhelm the host in order for its survival. Therefore, treatment regimens should be equally competent to outsmart these cells. Unfortunately, it is not the case with current therapeutic practices, the reason why it is still one of the most deadly adversaries and an imposing challenge to healthcare practitioners and researchers alike. With rapid nanotechnological interventions in the medical arena, the amalgamation of diagnostic and therapeutic functionalities into a single platform, theranostics provides a never before experienced hope of enhancing diagnostic accuracy and therapeutic efficiency. Additionally, the ability of these nanotheranostic agents to perform their actions on-demand, i.e. can be controlled by external stimulus such as light, magnetic field, sound waves and radiation has cemented their position as next generation anti-cancer candidates. Numerous reports exist of such stimuli-responsive theranostic nanomaterials against cancer, but few have broken through to clinical trials, let alone clinical practice. This review sheds light on the pros and cons of a few such theranostic nanomaterials, especially inorganic nanomaterials which do not require any additional chemical moieties to initiate the stimulus. The review will primarily focus on preclinical and clinical trial approved theranostic agents alone, describing their success or failure in the respective stages.

Contents

* Corresponding authors at: Bio-Nano Electronics Research Centre, Toyo University, Kawagoe, 350-8585, Japan.
E-mail addresses: maekawa@toyo.jp (T. Maekawa), sakthi@toyo.jp (S.K. D.).

https://doi.org/10.1016/j.addr.2018.10.007
0169-409X/

1. Introduction

Cancer ranks among the primary causes of death worldwide, with an ever-increasing incidence and mortality rate. Extensive basic and clinical investigations have portrayed cancer as a complex condition composed of malignant and normal cell types, which is one reason for the limitation of current single modality treatments against highly heterogenous early stage and advanced tumors [1–4]. Therefore, the combination of surgery, radio-, chemo- and immuno-therapies is inevitable under current clinical scenario. Unfortunately, patient heterogeneity and cancer resistance towards different modes of treatments results in poor therapeutic outcomes, leaving the patients with severe side effects from the treatment itself [5,6]. Thus, it is of prime importance to optimize patient-specific therapeutic regimes to achieve highest efficiency and results.

Rapid nanotechnological advancement in medical sciences has broadened our understanding with regard to subcellular and molecular cancer pathologies, facilitating the development of a large trove of custom-designed nanocarrier platforms including, but not limited to liposomal, dendrimeric, polymeric and inorganic nanoparticles (NPs) composed of metals and their oxides, quantum materials and related metal frameworks [7–10]. These nanomaterials have proven their potential in delivery of therapeutic molecules and other desired cargo, most of the time exactly to the target regions. Also, they have been employed as depots and carriers for various payloads, including hydrophobic entities, thereby improving the pharmacokinetics and enhance their stability and retention in blood, in addition to minimizing undesired side effects by providing options for cell/tissue specific delivery [11,12]. Such nano-theranostic (therapy + diagnosis) probes capable of detecting and locating tumors that can monitor and regulate treatment response have high appeal [13]. Interestingly, a special class of highly promising stimuli-responsive 'smart' nano-theranostic probes have recently emerged, distinguishing themselves from conventional nanomaterials due to their signature trigger-responsive ability [14]. The 'stimulus' or 'trigger' is a force which initiates a cascade of events, utilizing the nanomaterial's intrinsic or other organic/inorganic moiety assisted unique property, which in turn could be employed for applications as diagnostic imaging, therapeutics or both simultaneously. These triggers could be part of the cell/tumor microenvironment (intrinsic) or externally generated physical stimulus, with the latter offering superior spatiotemporal control of acquisition features and nanoprobe monitor [15–20]. These unique materials have been gaining extensive attention from the scientific research and medical community, especially owing to their remote-controllable multifunctional abilities.

Though numerous examples of nanomaterial based therapeutic interventions exist, here we discuss external stimuli-responsive multifunctional inorganic nanomaterials, for cancer theranostics (Scheme 1). The term 'external stimuli' in this review deals with light, magnetic field, ultrasound, radiofrequency and radiation (X-rays and gamma rays). These materials integrate 'controlled' imaging and therapeutic modules into a solitary platform, which is a revolutionary advancement in the path towards highly safe and effective personalized medicine. We provide a detailed account on external stimuli responsive nanotheranostics that are currently in clinic or under clinical/preclinical stages and aim for this review to be a collective archive of the most recent progresses in the specified field.

2. Concept of stimuli responsive nanotheranostics

Although their clinical applications are still in the early stages, when compared with conventional chemotherapy, numerous extensive preclinical studies employing the stimulus-responsive strategies have been shown to impart better therapeutic efficacy and limited side-effects [21]. As earlier discussed, specific triggers/stimuli can be broadly classified under intrinsic- and external-stimuli. 'Intrinsic-stimuli', are restricted to inside body/organism system, with the tumor microenvironment being an apt example for inducing local stimuli such as pH or interstitial pressure etc. Another set of parameters apart from the host's internal system, termed as 'external-stimuli' such as magnetic field, ultrasound, light, etc. exist [22]. Such modules demonstrate the ability to specifically initiate and control the therapeutic effects in the target region (e.g. tumor) with no or minimal effects to adjacent cells/tissues or organs. Also, certain physical stimuli such as applied magnetic field can aid in enrichment of nanoprobes specifically in the tumor region resulting in enhanced and localized effects [23]. Most forms of physical stimuli are able to control nanoprobe internalization and drug release/distribution in the tumor, thereby greatly improving the drug efficacy in addition to reducing their systemic toxicity. The effects of these materials are not only limited to direct cancer cell death, but can concomitantly trigger or boost other allied anti-cancer therapies resulting in highly effective and multidimensional, synergistic effects (e.g. by altering the tumor microenvironment). Utilizing such unique features of these nanomaterials, a range of physical-stimuli activated studies have been performed.

Photo-induced theranostics, employing photons or light to image/kill cancer is an extensively explored theranostic module. In such photo-stimuli strategies, conversion of light energy into either heat or singlet oxygen ($^1O_2$)/reactive oxygen species (ROS) occurs by specific wavelength light absorbing agents or photosensitizer molecules, respectively. In addition, the stimuli can also serve in imaging of tissues, viz. optical imaging [24]. Another widely used physical trigger, magnetic field (MF) is utilized to stimulate magnetic nanomaterials, which can generate heat under an oscillating MF, or be magnetically directed to lesion sites. Additionally, a widely utilized application of MF stimuli is for magnetic resonance imaging (MRI) of tumor tissue [25,26]. Ultrasound (US) is another mode of stimulus which has been used to trigger site-

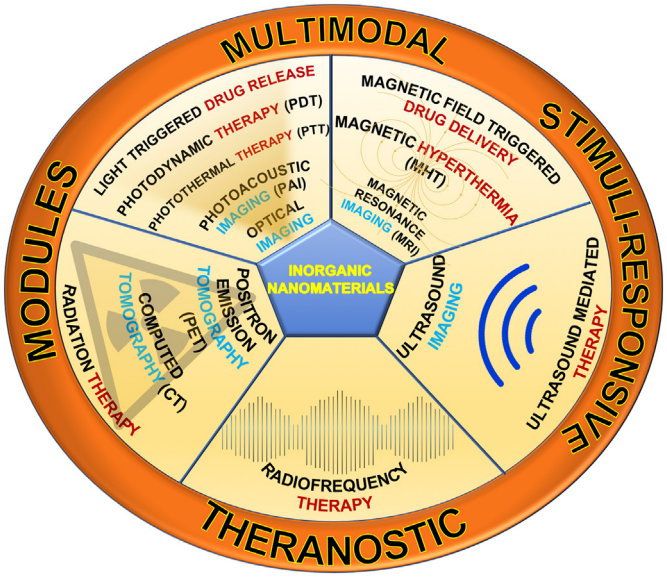

Scheme 1. Multimodal applications of inorganic nanomaterials as stimuli-responsive theranostic agents.

specific therapeutic agent delivery, often utilizing the micro-bubble (MB) technology [27,28]. Like MF, ultrasound has also been well established as a mode of imaging under clinical scenario. Longer wavelength radiofrequency (RF), and shorter wavelength X-rays, have also been investigate as stimuli for cancer therapy as well as diagnosis with help of specially designed nanoagents [29,30]. The general mode of action of stimuli-responsive systems would include the intravenous (I.V.) (or other administration mode like intraperitoneal (I.P.)), injection of the theranostic probe, which passively accumulates in the tumor region by neovascular leakage utilizing the enhanced permeability and retention effect (EPR). On the other hand, active targeting based on the receptor-ligand affinity principle, could also be used for more specific and preferential tumor accumulation. Once target site is reached, passively/actively, the probes are activated with single or several external triggers to induce desired theranostic outcomes, that can range from release of therapeutic agents (on-demand/controlled drug release), alternative therapies (thermal, ROS generation etc.) to imaging. Detailed explanation with suitable examples for each mode of stimulus and responsive materials is provided herein.

3. Light responsive theranostics

The ease of control and utilization, apart from the spatiotemporal control of nanoprobes, allows light to act as an effective external trigger/stimulus [31]. Unfortunately, the major issue of finite tissue penetration in this mode severely restricts the use against tumors that are located deep in tissues. The NIR region (650 to 900 nm) is regarded as the 'biological window' as most of the body components such as blood and soft tissues are transparent (do not absorb or scatter light) in this wavelength region, thus granting access to non-invasive, deep tissue penetration for imaging and therapeutic purpose. Due to reasons such as wide clinical application in tumor imaging, photosensitizers (PSs) based cancer killing (local hyperthermia, ROS or $^1O_2$) and features such as high spatiotemporal precision, real-time dose control adjustment along with the option for on demand switching on and off modes, have generated high expectation for the light stimulus triggered theranostics.

Heat and $^1O_2$ generation are two of the most critical effectors in this mode of therapy. Hyperthermia (HT) effectuated due to heat generated by the PSs resulting in cell death is known as photothermal therapy (PTT). Elevating the tumor microenvironment temperature to 42 °C can not only induce cellular damage, but also render vulnerability to cancer cells to allied treatments such as irradiation and chemotherapy. A further temperature increase to 45 °C or above would exert immediate lethal effects on the cells, negating the need for additional therapies. $^1O_2$ is responsible for causing irreversible damage to intracellular organelles, also known as photodynamic therapy (PDT). Interestingly, the extremely short lifespan (<3.5 μs) and highly restricted diffusion (~10 to 20 nm) of $^1O_2$ can be exploited for localized apoptosis, necrosis, or autophagy induced cell death [32–35]. Likewise, light-triggered controlled and localized drug release can also be achieved, leading to site-specific therapy [36]. Apart from these therapeutic aspects, the light-based imaging techniques as fluorescence, photoacoustic (PA) signal and Surface Enhanced Raman Scattering (SERS) are useful in live bioimaging [37–39]. This section will mainly focus on the use of light-stimulated theranostic nanoprobes, currently in pre-clinical and clinical stages.

3.1. Photothermal therapy

Lasers, continuous wave or pulsed, play a central role in PTT by irradiating the cancer cells/tissue with an electromagnetic radiation (e.g. visible or NIR) causing a rapid temperature spike, wherein the incident light energy is converted to heat (45-300^{0}C), resulting in cell death via varied mechanisms. In the case of continuous wave lasers, constant blood perfusion in the target tissue causes notable heat loss, therefore diluting the HT effect and necessitating the requirement for adequate energy to compensate the loss in thermal efficiency. On the contrary, pulsed lasers, with a shorter pulse width than the normal thermal relaxation time of tissues, can induce acute thermal confinement in the targeted tissue, leading to severe necrosis. Tuning the laser parameters and focusing on the target region allows for the sensitization of PSs and execute the desired imaging or therapeutic effect precisely at the lesion, so as not to disrupt surrounding cells/tissues [40,41].

A vast array of inorganic NPs have been developed for theranostic applications involving light which include gold (Au) nanostructures, carbon nanomaterials, 2D nanomaterials, semiconductors etc. [42–49]. One example is of Polyethylene glycol (PEG)-tumor necrosis factor-α-coated Au NPs (CYT-6091) which were able to decrease the interstitial tumor fluid pressure in a 4T1 murine breast tumor model apart from curbing the growth of tumors in a SCCVII head and neck tumor model [42]. CYT-6091 from Cytimmune, a formulation of rhTNF functionalized PEGylated AuNPs (27 nm) was the first clinical trial product for advanced solid tumors bearing patients (NCT00356980) [50]. 30 patients were systemically administrated with CYT-6091 at a previously toxic dose of rhTNF. Analysis revealed the localization of Au in breast tumor tissue with absence in adjacent healthy tissue, highlighting the specificity of this formulation. To understand the vascular leak mechanisms and assess the safety and efficiency of CYT-6091, dynamic contrast-enhanced MRI is being employed, while Phase II clinical trials are underway [51].

An FDA-approved pilot study of AuroLase®, (silica-Au nanoshells coated with (PEG)) that can thermally ablate solid tumors on stimulation with NIR laser, for PTT (NCT00848042, NCT01679470) was conducted [52,53]. The Au shell performs the NIR-triggered thermal ablation while Si serves as the dielectric core, and PEG imparting overall particle stability and biocompatibility. The principle findings of this work, the technology for which was first reported 10 years back, showed that AuroLase® could induce irreversible thermal damage to tumors in mice. Furthermore, AuroLase® was tested for brain and prostate cancer treatment, with the latter succumbing to efficient and complete thermal ablation [54–56]. These studies paved way for two independent clinical trials, first of which (NCT00848042), was reportedly completed for patients with refractory and/or recurrent head and neck tumors [52]. The second trial, tested AuroLase® against primary or metastatic cancer derived advanced lung tumors, where additionally, the airway is obstructed. Though the trials are completed, results are as of yet awaited [53]. AuroLase® is concurrently being investigated as an allied therapy with RT [57] and imaging along with US-triggered focal ablation of prostrate lesions at the preclinical level [58]. With respect to the latter, AuroShell® particles were administered as single I. V. infusion, 12-36 hr prior to US-directed laser irradiation. Negative biopsies post therapy confirmed the efficient focal ablation of clinically significant prostate lesions with minimal healthy tissue damage (NCT02680535). NANOM FIM, another phase I\II clinical trial (NCT01270139) completed nanoplatform, based on Si-AuNPs (core-shell Si-AuNP and core-shell Si-AuNP iron), were recently revealed [59] that utilize plasmon photothermal strategy to treat atheroma. In another work, the efficacy of interventional PTT was investigated against clinical iodine-125 interstitial brachytherapy (IBT) in an orthotopic xenograft model of human pancreatic cancer. An anti-urokinase plasminogen activator receptor antibody, PEG, and indocyanine green (ICG) modified gold nanoshell system (uIGNs) was administered via local injection, followed by PTT (Fig. 1). Each treated lesion was monitored at 3-day intervals using bioluminescence imaging (BLI). Final observations revealed complete ablation of tumors in IPTT uIGN group, while all other groups had residual tumors. When compared to IBT-125-I, a 25% higher median survival rate was recorded in IPTT, where complete ablation of tumors was achieved by one-time intervention. This nanosystem based IPTT competently challenges the conventional treatment strategies and could be developed for translation to potential clinical setting as well [60].

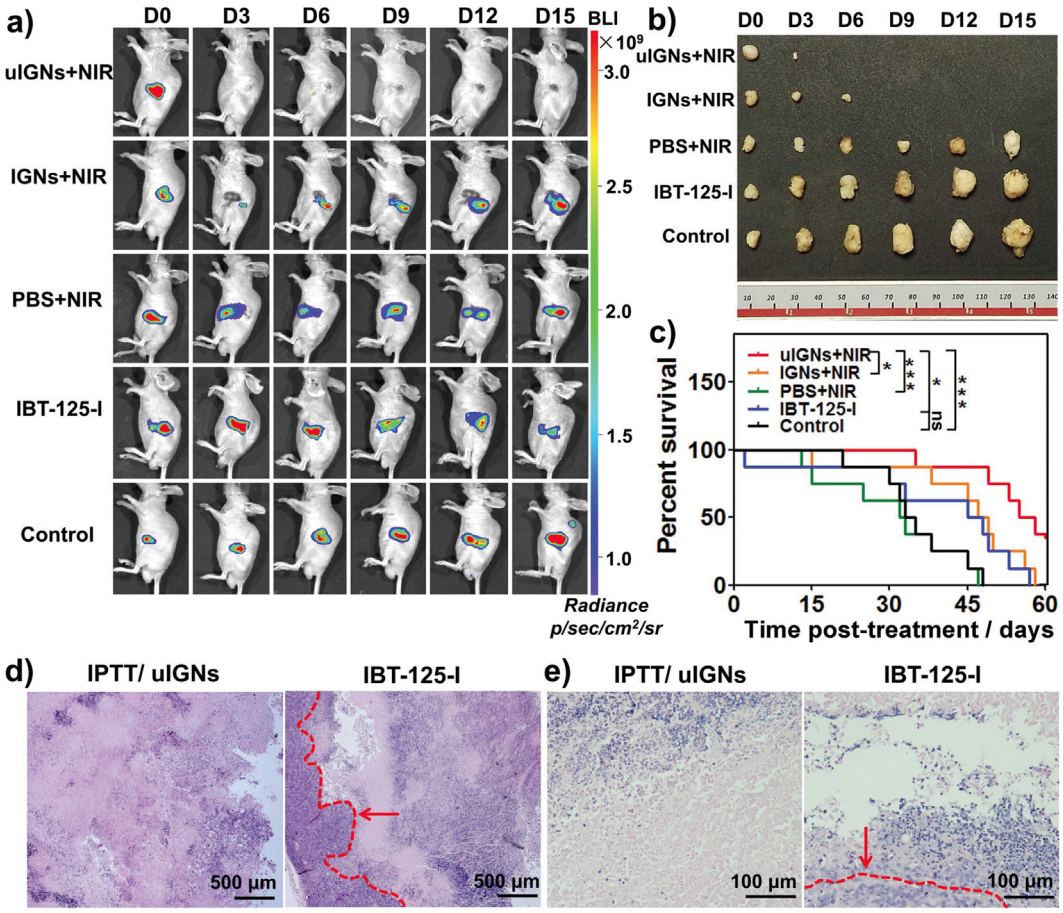

Fig. 1. Evaluation of the therapeutic effects. a) BLI was utilized to continuously monitor the treated lesions at 3 d interval in different groups. b) Photo images of the resected tumors in different treatment groups at 3 d interval. c) The mice in different groups were monitored for 60 d following treatment and percent survival was calculated. d,e) Tumor tissues treated by uIGN-mediated IPTT and IBT-125-I were resected post-treatment and H&E stain assay was performed. Large area of necrosis was observed in tumor tissues from both treatment groups, but residual live tumor cells were only observed in IBT-125-I treated tissues (circled by the dashed line and indicated by red arrow). Reproduced with permission [60].

One notable application of PTT was against the microscopic residual disease (MRD), which is responsible for the post-surgery tumor resurgence and metastases. A photomechanical product of photothermal triggering, Au based plasmonic nanobubbles (PNBs), have shown promise in in vivo, real-time intraoperative detection of MRD. The endocytosed AuNPs, induce transient, photomechanical vapor NBs when exposed to a short laser pulse. Here, rather than using the photothermal application for inducing cell death, it is employed for the production of PNBs, which in turn are used for MRD detection by releasing an acoustically recordable pressure pulse specifically from cancer cells which differs from normal tissues. Post resection of primary tumor mass, PNBs can locate MRD in real time, allowing for its removal till the signal persists. All of the animals (100%) in this treatment regime had no tumor relapse. However, neither false-positive nor -negative signals were recorded on PNBs application to Au pretreated head and neck squamous cell carcinoma (HNSCC). Interestingly, in such cases as unresectable MRD, the mechanical pulse created by PNBs is sufficient to destroy cancer cells. This phenomenon is dependent on the PNBs size which needs to be lethal enough, determined by the incident laser parameters, otherwise the method remains a diagnostic [61,62]. Hybrid structures like, Au nanorods (AuNRs) coated with a Pt nanodots shell, enhanced the photothermal effect than the free nanorods. This was primarily due to prevention of AuNRs aggregation by the Pt shell in the endosomal/lysosomal compartments, thus conserving the original sharp localized surface plasmon resonance (LSPR) of AuNRs [63]. Liu group used GO for the first time for in vivo PTT, subsequently improving the PTT effect further by using reduced GO (rGO), which exhibits a 7-fold increase of NIR absorbance than GO [64]. In certain cases, as Jiang et al. reported, hybrid structures as Au-Cu_9S_5 core/shell NPs can have higher PCE (37%), due to combination of Au and Cu in a single NP [65]. Similarly, Liu et al. fabricated hybrid, sub-10 nm Fe_3O_4@$Cu_{2-x}S$ core-shell NPs with maximum absorption at ~ 960 nm, and accurate control of PCE by simply tuning the concentration of Cu [66].

3.2. Photodynamic therapy

PDT is fast emerging as a highly promising cancer treatment option, with organic/inorganic photosensitizers being its fundamental tools. PSs, upon laser exposure, transfer the absorbed energy to adjacent molecular oxygen, causing formation of ROS (e.g. $^1O_2$) or free radicals, which initiate apoptosis resulting in death of diseased tissue. While PTT requires higher laser power intensity to induce hyperthermia, PDT uses much lower light intensity for cell death. Other highlights of PDT are its negligible invasiveness, lower damage to hemopoietic and immune system and lower toxicity incidences culminating in safer treatment option for patients. An ideal PS is expected to possess negligible dark-toxicity, high quantum yield of triplet state formation with relevant triplet lifetime for interaction with ground state oxygen for the generation of ROS. However, many PSs, especially organic PSs, suffer from lack of tumor selectivity, toxicity, photodegradation/sensitivity and a maxima absorption above 700 nm. Recent years have seen a steady emergence of inorganic nanomaterials serving as PSs, which claim to overcome the drawbacks of conventional organic PSs [67–72].

Upconversion NPs (UCNPs) owing to their large anti-Stokes shifts, deep tissue penetration, narrow band emission, and high

spatiotemporal resolution, have found extensive use in imaging and PDT [73,74]. Conventional UCNPs have excitation at 980 nm, similar to where water has significant absorption, raising concerns that the cell killing could be due to overheating effect. Alternatively, $NaYbF_4$:Nd@$NaGdF_4$:Yb/Er@$NaGdF_4$ core-shell-shell NPs loaded with Chlorin e6 and folic acid was synthesized for synchronous imaging and PDT. The excitation wavelength of 808 nm for the NPs negates the absorption of water thus facilitating high energy transfer efficiency and generation of cytotoxic $^1O_2$. Moreover, the efficient $^1O_2$ generation beneath 15-mm thick muscle tissue highlighted the higher penetration depth of this system, implying its ability to effectively terminate intrinsic tumors or core of larger tumors through PDT [75]. Another potential PDT candidate is titanium dioxide (TiO_2) which exhibits minimal dark cytotoxicity complemented by its excellent responsiveness to ultraviolet (UV) light for inducing cytotoxicity, however suffers from the conventional drawback of restricted tissue penetration of UV light. Therefore, an NIR light activated core/shell nanocomposite of UCNP and TiO_2 nanocrystals (UCNPs@TiO_2 NCs) were designed where, $NaYF_4$:Yb^{3+},Tm^{3+}@$NaGdF_4$:Yb^{3+} core/shell UCNPs competently generate UV emission from NIR light by converting the latter to shorter wavelength light, correlating with the absorption of TiO_2 shell. These UCNPs@TiO_2 NCs, upon NIR light trigger, are able to generate intracellular ROS resulting in disrupted mitochondrial membrane potential that sequentially induces apoptosis. Utilization of NIR light for the activation of UCNPs@TiO_2 provides better tissue penetration than UV irradiation and better PDT of tumor-bearing mice [76]. In another work, folic acid (FA)-modified $NaGdF_4$:Yb/Tm@SiO_2@TiO_2 nanocomposites (FA-Gd-Si-Ti NPs) were developed for MRI and NIR-responsive inorganic PDT, where NIR light could excite TiO_2 thanks to the upconversion light (UCL) performance of $NaGdF_4$:Yb/Tm which convert NIR to UV light. These nanocomposites showed good biocompatibility and were efficient T1-weighted MRI (T1-W MRI) contrast agents with bright signals at xenografted tumor site in nude mice (longitudinal relaxivity (r1)=4.53 $mm^{-1}s^{-1}$). Furthermore, PDT of MCF-7 breast cancer tumor-bearing mice showed nearly 88.6% tumor inhibition after a 2-week treatment regime [77]. Meanwhile, another class of biocompatible UCNPs was developed with highly amplified red-emissions, a 15-fold stronger absolute upconversion quantum yield (3.2%) than conventional β-phase core/shell UCNPs. Significant PDT effect in deep-tissue (>1.2 cm) tumors was experienced, on conjugating aminolevulinic acid (5-ALA), a clinically approved PDT prodrug that requires red light excitation, to the UCNPs. Furthermore, the NIR based UCNP-PDT system clearly outperformed the clinically used red light irradiation, thus signifying the utilization of UCNPs to effectively access and induce PDT in deep seated tumors when compared to excitation of conventional PS alone. These findings reveal the potential for a wider application of UCNPs in upconverting red radiation in photonics and biophotonics [78]. Subsequently, a dual therapeutic nanocomposite, doxorubicin (DOX)-loaded $NaYF_4$:Yb/Tm-TiO_2 (FA-NPs-DOX) was synthesized for NIR-stimulated PDT and DOX-mediated chemotherapy against multidrug resistant (MDR) breast cancers. FA-mediated targeting alleviated cellular uptake of NPs followed by ROS generation from TiO_2 inorganic PSs under 980 nm laser irradiation, utilizing the UCL performance of $NaYF_4$:Yb/Tm. Accelerated release of DOX was achieved resulting in an inhibition rate of 90.33% in the drug-resistant MCF-7/ADR tumors, compared to free DOX, highlighting the dual mode therapeutic efficiency of augmented chemotherapy and NIR-mediated inorganic PDT by the nanocomposites [79]. Another example of NIR light triggered PDT based on a hybrid multifunctional nanoconstruct comprising of UCNPs and a PS zinc(II) phthalocyanine (ZnPc) was reported. ZnPc were anchored close to the UCNPs by a folate-modified amphiphilic chitosan coating on the latter, to facilitate resonance energy transfer from UCNPs to ZnPc. Higher ROS generation, under a 1cm tissue, was observed on 980 nm light excitation of UCNPs than with 660 nm irradiation of ZnPc. In vivo NIR-PDT of deep-seated tumors demonstrated a 50% tumor inhibition ratio compared to conventional visible light-triggered PDT (tumor inhibition ratio of 18%) [80].

Other inorganic nanomaterials, apart from UCNPs have also recently been reported for PDT. Copper sulfide ($Cu_{2-x}S$) NCs, due to their plasmonic nature have gained considerable attention as materials for PTT. Earlier reports have linked the photoinduced cell death to photothermal heat generation by these NCs, with lack of any direct proof of their photodynamic properties. Interestingly, it was observed that apart from the high PTT efficacy, these $Cu_{2-x}S$ NCs could also generate high levels of ROS on NIR-activation, which were observed under both in vitro and in vivo scenarios [81]. Similarly, Au nanoshells, which have been studied for their NIR-induced thermal competency were also observed to perform PDT, apart from fluorescence emission and sensitizing formation of $^1O_2$. Fluorescence emission spectra and DPBF quenching studies confirmed NIR photoirradiation induced $^1O_2$ generation. It was observed that Au nanoshells mostly exert PDT upon low dose (~150 mW/cm^2) 980 nm irradiation to suppress B16F0 melanoma tumors and demonstrating the nanoconstructs's multi-functional theranostic potential (fluorescence imaging/PDT/PTT) [82]. Similarly, poly(acrylic acid) (PAA)-coated $Cu_2(OH)PO_4$ quantum dots (QDs), exhibiting strong NIR photoabsorption and excellent PCE were developed, which could induce the photoactivated formation of ROS (PDT) and PTT as well. In vivo phototherapeutic analysis of solid tumors demonstrated significant antitumor effects of $Cu_2(OH)PO_4$@PAA upon 1064-nm laser excitation, without any adverse effects on normal tissues and organs. $Cu_2(OH)PO_4$@PAA additionally provides NIR irradiated photoacoustic tomography (PAT) imaging contrats to visualize tumors and thus serve as multifunctional theranostic platform [83].

3.3. Light-triggered drug delivery

Apart from the two strategies mentioned above (PTT/PDT), light-sensitive materials are being widely acknowledged as on-demand drug delivery and release agents. Light-responsive drug release systems have been fabricated employing such mechanisms as, photoisomerization, photocrosslinking/decrosslinking, photosensitized oxidation, light-triggered polarity switching, photo- or photodegradation of the polymer backbone [84]. As explained earlier, the limited tissue penetration of 600-700 nm light, which is the working range of most PSs used for PDT, is a major drawback. Also, as previously mentioned, UCNPs can absorb light greater than 800 nm but emit visible or NIR light with narrow bandwidth. Utilizing this phenomenon in chemotherapy, a multifunctional UCNPs system with mPEG-COOH, PS Ce6 and ROS-cleavable thioketal-conjugated camptothecin (CPT) was formulated. UCNPs, at 980 nm laser irradiation convert light to 645–675 nm region, thus exciting the PS Ce6 and inducing ROS generation for PDT, while simultaneously cleaving the thioketal-CPT linker for effectuating chemotherapy. Also, the activated Ce6 can be used for imaging based on its fluorescence emission. Unlike smaller organic dye candidates, the conjugated polyelectrolytes' (CPEs) backbone can harbor enough light absorbing units, responsible for laser-stimulated high absorption coefficient resultant fluorescence. The combination of CPEs that can produce ROS and cleave thioketal groups releasing the anticancer drug DOX simultaneously, form an efficient controllable light-stimulated ROS responsive drug delivery/PDT system [85]. Cholesteryl succinyl silane (CSS) nanomicelles encapsulating DOX, Fe_3O_4 magnetic NPs, and Au nanoshells were fabricated as a multi-component/functional drug-delivery system. These composite nanomicelles exhibit an 808 nm NIR laser-induced temperature increase which also results in gradual DOX release. The T_m value of these CSS nanomicelles is high, thus requiring high temperature for its destabilization. This is particularly beneficial when considering the on-demand release of DOX only upon NIR irradiation of the Au nanoshells which in turn would elevate the local temperature, loosening the micelles and effecting drug release, thereby minimizing undesired leakage of drug during circulation [86]. In another work, DOX loaded, PEGylated mesoporous Si (MS) coated

single-walled carbon nanotubes (SWNTs), SWNT@MS-PEG were employed for NIR-triggered PTT and associated DOX release to create a synergistic dual-mode anti-cancer therapy [87]. Au-based NPs that absorb NIR light have shown the potential to selectively target and treat cancer through highly efficient light-to-heat conversion. In another example, NIR light-triggered release of docetaxel from an Au nanoshell-based DNA host complex, and lapatinib from nanoshell-based DNA and human serum albumin host complexes, was demonstrated. Localizing drug delivery, both spatially and temporally by combining Au nanoshell-based complexes and pulsed-laser irradiation was proven in this work leading to highly controlled drug delivery that can apply to a myriad of therapeutic applications [88].

3.4. Optical imaging

Optical imaging is a significant, convenient and powerful technique that relies on fluorescent probes to record information of biological entities ranging from individual cells to tissues and organs. With hallmarks as obvious image contrast, fast response, high sensitivity, controllable targeting and minimal damage to healthy tissues, it has been under extensive use for diagnosing malignancies or drug distribution and metabolism monitoring. Taking into consideration that some biological entities as blood show visible region auto/self-fluorescence, fluorescent probes are designed with strong NIR region (700–1400 nm) absorbance to avoid any overlap. Compared with NIR fluorescent organic dyes (cyanine, rhodamine, squarain etc.), NIR-light-emitting inorganic NPs are endowed with considerably higher colloidal and photo stability in addition to superior blood longevity [89,90]. Among these, UCNPs due to their NIR-triggered non-blinking visible emission and excellent photostability exhibit high resolution UCL imaging. A range of UCNPs have been manufactured for application in UCL optical image-guided cancer therapy [91]. For example, $NaYbF_4$:Er UCNPs were developed for similar purpose. Apart from the fluorescence imaging and cancer therapy potential, due to the presence of Yb, the NPs also have strong X-ray attenuation ability and thus function as a multimodal theranostic system[92]. Few metallic NPs such as Au nanocrystals (AuNCs) have drawn great interest recently due to their excellent fluorescence property. Small AuNCs (<2 nm) have displayed ultrabright fluorescence, low toxicity, and high photostability, features which could be exploited in in vivo imaging. Feng et al., developed advanced theranostic micelles by incorporating transferrin (tumor targeting), docetaxel (therapy) and AuNCs resulting in significant tumor accumulation, excellent tumor killing accompanied with enhanced fluorescence imaging [93].

QDs have also been extensively investigated as potential bioimaging agents. Conventional II-VI type semiconductor crystalline QDs (i. e. CdSe), despite their bright fluorescence, have shown toxic tendencies due to the present of heavy metals. Meanwhile, certain fluorescent QDs devoid of heavy metals such as fluorescent CDs, have exhibited wavelength-dependent luminescence, commendable biocompatibility and low toxicity profile making for promising theranostic agents [94]. Similarly, another member of carbonaceous nanomaterial family, graphene QDs (GQDs), with excellent photoluminescence properties, have also been investigated as a PSs for PDT in recent years [95]. Usually, IR based fluorescence imaging was performed in the 1st NIR window (NIR-I, 700–1000 nm), with weak sensitivity and signal to-noise ratio and more importantly shallow tissue penetration. Incidentally, QDs with emission in the 2nd NIR window (NIR-II, 1000–1400 nm) have been recently explored as alternatives. Ag_2S QDs are a good example of NIR-II QDs, with high tissue invasion, bright fluorescence, good spatiotemporal resolution and blood longevity. Wang et al. designed PEGylated Ag_2S QDs for the real-time detection and visualization of early-stage tumors (Fig. 2) where the tumor contour and vascular microstructures were precisely recorded, along with monitoring real-time drug release and tumor therapy [96]. Another prospective high sensitivity imaging modality, SERS, derives significantly enhanced Raman signals from biomolecules adsorbed on some noble metals. Owing to their strong LSPR, remarkable physico-chemical stability, facile surface modification and good biocompatibility, Au nanostructures are widely investigated and applied as SERS substrates [97]. A colloidally stable, high drug load yolk-shell Au-based nanoplatform (AuNR@void@$mTiO_2$ NPs) was designed by Zhang et al., for real-time SERS imaging-based theranostics. Compared to spherical AuNPs, differently shaped AuNPs provided better imaging due to their strong SPR in the NIR region, having great potential in deep tissue applications [98].

3.5. Photoacoustic imaging

PAI utilizes the acoustic wave signals generated by the transient thermoelastic expansion of target tissues due to absorption of non-ionizing laser pulse. It can detect the hemoglobin oxygenation state, as the ultrasonic emission intensity and the signature optical absorption contrasts for different biological tissues are proportional. High absorption of PAI agents is directly proportional to the thermal generation, which can be used for high specificity tumor ablation [99,100]. Au nanomaterials have been favorites as PAI agents for their tunable optical properties and acceptable signal-to-noise ratio [101]. Ye et al. demonstrated the excellent enhancement of PA signals from AuNTs (300–700 nm) under high efficiency NIR-SPR mode excitation, facilitating the easy observation of AuNTs' EPR mediated accumulation in tumors [102]. Another work utilized red emitting CDs (500 to 800 nm with peak at 640 nm) with high PCE ($\eta = 38.5\%$) for multimodal fluorescence/PAI and thermal (PTT) theranostics [103]. Song et al., developed novel AuNR vesicles (~60 nm) from small AuNRs (~8 × 2 nm) functionalized with PEG and PLGA for image-guided PTT of cancer. The AuNR@PEG/PLGA vesicles degrade into small hydrophilic AuNR@PEG due to hydrolysis of PLGA. The robust interparticle plasmonic coupling greatly enhances the PCE and PA signal of AuNR vesicles in comparison with AuNRs. Prominent tumor uptake of I.V. injected AuNR vesicles to U87MG tumor mice was observed with strong PA signals from the target site, confirmed by continuous enhancement of 2D and 3D PA images and intensities over time [104]. A major obstacle towards better brain tumor therapy in patients is the delineating of tumor margins from normal tissue, aided by the weak sensitivity, specificity, and spatial resolution of current imaging methods. To address this issue, Kircher et al., synthesized unique triple-modality picomolar sensitivity MRI-PA-SERS NPs (MPR) that could accurately delineate the brain tumor boundaries in mice both pre- and intra-operatively (Fig. 3). I.V. injection of MPRs to glioblastoma (GBM)-bearing mice caused the MPRs to specifically accumulate in the tumors, facilitating for MRI-PA-SERS modalities mediated non-invasive tumor demarcation through the intact skull. Raman imaging assisted intra-operative tumor resection, and subsequent histological observations validated the accuracy of SERS in delineating brain tumor margins [105]. In another work, CuS loaded Cy5.5-conjugated hyaluronic acid NPs (HANP) was developed for theranostic purpose. Degradation of the tumor-internalized composite by hyaluronidase leads to bright Cy5.5 fluorescence, delineating the tumor from surrounding tissue. Post I.V. administration to SCC7 tumor-bearing mice, prominent fluorescence and PA signals were recorded from the tumor over time, with a signal maxima at 6 h with tumor-to-normal tissue ratio of 3.25 for optical and 3.8 for PA imaging. Tumor irradiation with an NIR laser resulted in highly efficient inhibition (89.74% on day 5) [106].

4. Magnetic responsive theranostics

Magnetic NPs (MNPs), due to their unique intrinsic properties, have been receiving much attention for their magnetic responsive enhanced applications in the biomedical field, most renowned being MRI. Unlike optical modules, magnetic fields at frequencies below 400 Hz, are not readily absorbed by tissues, granting remote monitoring/manipulation without physical contact. MNPs, on stimulation with permanent or

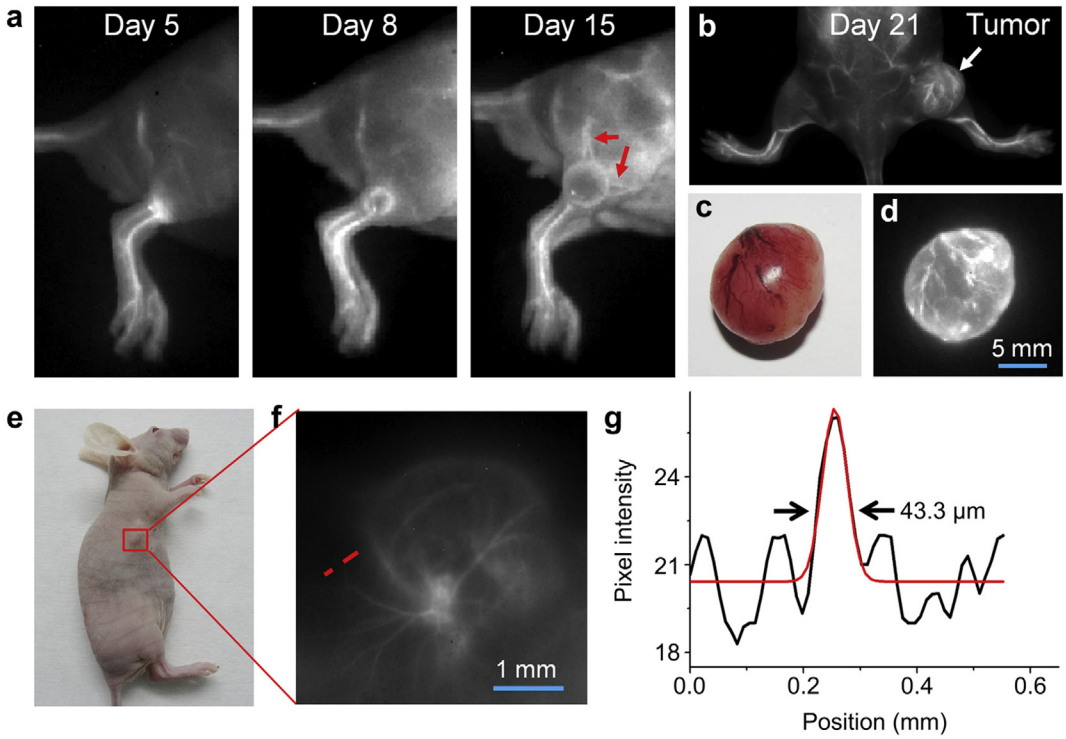

Fig. 2. In vivo real-time visualization of tumor-induced angiogenesis. NIR-II fluorescence images of the 4T1 mammary tumor-bearing mouse. Fluorescence images were acquired after 30 min post I.V. injection of PEGylated Ag_2S QDs (1 mg/mL, 200 mL) on day 5, 8, 15 (a) and 21 (b) after 4T1 tumor transplantation, respectively. Red arrow unambiguously visualized the tumor-induced angiogenesis in vivo with the help of NIR-II PEGylated Ag_2S QDs, whereas the white arrow located the 4T1 tumor. (c) Daylight image of the tumor extracted from mouse. (d) NIR-II fluorescence image of the tumor. (e) Color photo of U87MG tumor-bearing mouse. (f) Amplified fluorescent image of the selected region in (e). (g) A cross-sectional intensity profile measured along the red-dashed line in (f) with its peak fitted to Gaussian functions. Reproduced with permission [96].

alternating magnetic fields (PMF/AMF) can be employed for remotely-controlled drug delivery, HT and imaging-guided therapy [107,108].

4.1. Magnetic hyperthermia (MHT)

Thermal ablation is emerging as one of the most reported types of therapy for solid tumors and super paramagnetic iron oxide NPs (SPIONs) have been extensively researched in this regard. HT therapy applying iron oxide NPs (IONPs) involves administration of an IONPs fluid to the tumor, with subsequent AMF application, which effectuates NPs heating and consequent ablation. A temperature rise of 41- 46 °C can impart severe effects to both cells and tissues, as a result of heat stress induced higher heat-shock protein expression, protein denaturation/folding and apoptosis. Specifically in tissues, the temperature spike promotes pH change, perfusion and oxygenation of the tumor microenvironment, with persistent higher temperature leading to necrosis [109–111].

Clinical studies on HT using IONPs for prostate cancer and GBM patients were commenced in 2007 (NCT02033447 and DRKS00005476) [112,113]. Johannsen et al. transperineally administered IONPs fluid into the prostate of 10 patients followed by 6 thermal therapies of 60 min duration at weekly intervals. A maximum temperature of 55°C was achieved in the prostate, median tumor temperature being 40.7°C and 40.2°C in peritumoral zones. Eventually, another clinical study explained the concept of interstitial heating of IONPs which was well tolerated in locally recurrent prostate cancer patients. The study also revealed the highly durable deposition of NPs in the prostate [114]. Parallelly, Maier-Hauff et al. investigated the effects and tolerant levels of thermotherapy in recurrent GBM patients. 4 - 10 thermotherapy cycles were conducted, with a 44.6 °C median intratumoural temperature (Fig. 4) and it was concluded that IONPs-thermotherapy was well-tolerated by individuals with minimal to no side effects. A clinical study conducted few years later revealed a median overall survival of 13.4 months post-diagnosis of first tumor recurrence, which was a commendable enhancement to the 6.2 months in other reference studies and the median overall survival after primary tumor diagnosis was 23.2 months, compared with just 14.6 in the reference groups [115].

More recently, HT was employed by Matsumine et al. in metastatic bone tumor patients. A composition of 'Bare' magnetite NPs and calcium phosphate cement, a biocompatible bone substitute, were implanted following initial surgical intervention. A 15 min therapy was given to patients every alternate day, beginning on the 8th day post-surgery. Results indicated a lesion reduction of 32% with visible bone formation, while 64% were devoid of any progressive lesions for a period beyond 3 months and only 4% had negative therapeutic response [116]. Although promising, development of MHT therapies are still in infancy and extensive research at the preclinical and clinical level need to be performed for its approval as a standard of care treatment. Also, questions regarding the distribution of IONPs with MHT, and peritumoural tissue damage, need to be thoroughly assessed. To answer these issues, a phase 0 clinical trial regarding the MNP thermo-ablation-retention and maintenance in the prostate was carried out by University College London Hospitals (NCT02033447). The study is to govern the actual location of MNPs and track them from the injected site through to sensitive regions surrounding the prostate. Meanwhile, a new open-label, randomized clinical trial is being conducted by MagForce, employing MHT to treat GBM patients (DRKS00005476). The trial, proposed to enroll ~285 patients, is being conducted to assess the practicability and safety of MHT as an independent or combination (RT) therapy employing NanoTherm®, commercial IONPs. Recently, PEGylated magnetite NPs, intratumorally injected into epidermoid carcinoma xenograft mice were able to restrict tumor growth via MHT. The different timepoint thermographic IR data taken during MHT exhibited increased temperatures in the tumor site injected with NPs whereas no such temperature rise were recorded from other regions. An interesting observation was that the heating capacity of these NPs was considerably

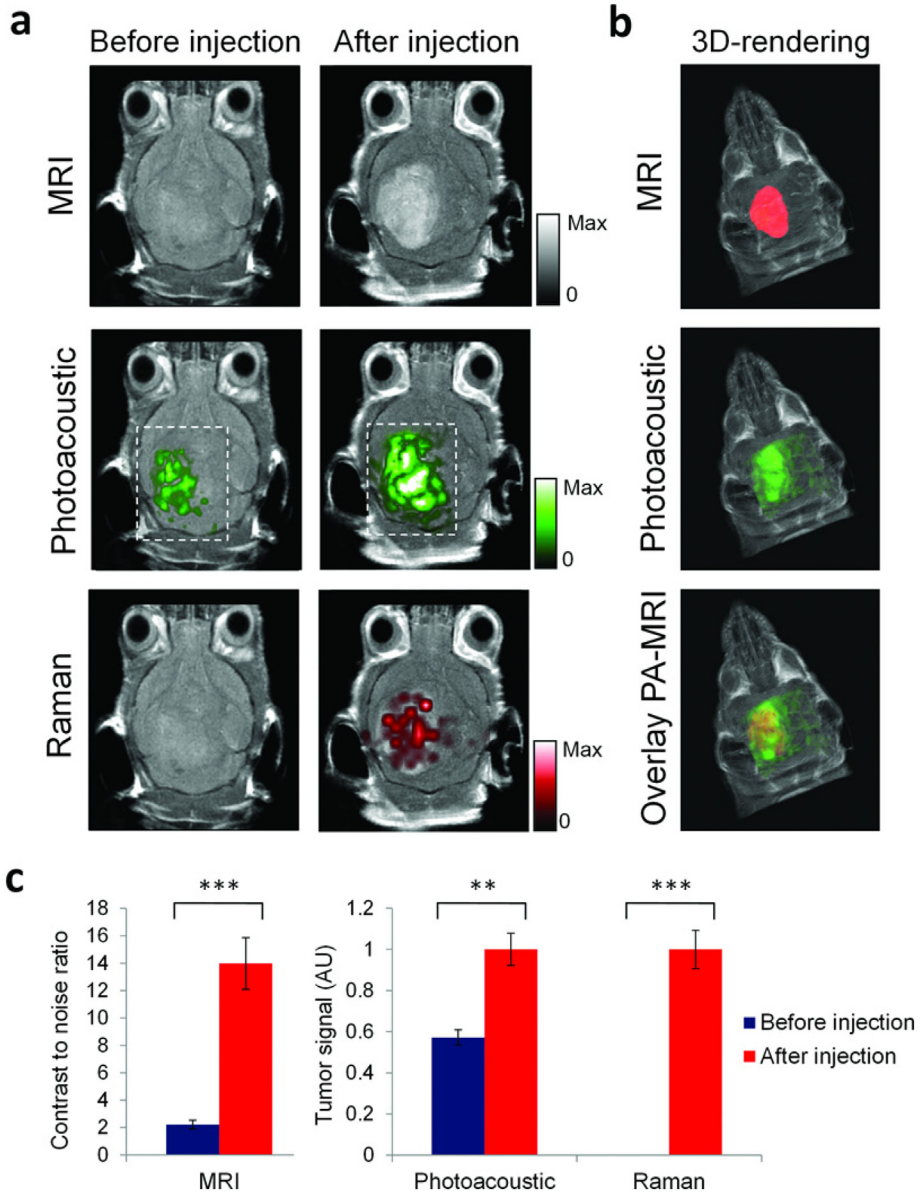

Fig. 3. Triple-modality detection of brain tumors in live mice with MPRs. Three weeks after orthotopic inoculation, tumor-bearing mice (n = 4) were injected I.V. with MPRs (16 nM, 170 μl). PA, Raman and MRI of the brain (skin and skull intact) were acquired before and 2 h, 3 h and 4 h after injection, respectively. (a) 2D axial MRI, PA and Raman images. The post-injection images of all three modalities demonstrated clear tumor visualization. The PA and Raman images were co-registered with the MR image, demonstrating good co-localization between the three modalities. (b) 3D-rendering of MR images with the tumor segmented (red; top); overlay of 3D PA images (green) over MRI (middle); and overlay of MRI, segmented tumor and PA image (bottom) showing good co-localization of the PA signal with the tumor. c. Quantification of signal in the tumor shows significant increase in MRI, PA and Raman signals before versus after the injection ("****" indicates $P < 0.001$, "**" indicates $P < 0.01$). Error bars represent s.e.m. AU, arbitrary units. Reproduced with permission [105].

diminished upon cellular internalization but had good effect in the interstitial extracellular space. Besides, the MHT-induced extracellular matrix destruction increased the drug penetration as was documented by the excellent curb on tumor progresssion [117].

4.2. Magnetic resonance imaging

MRI is an indispensable medical diagnostics tool, offering non-invasive, detailed real-time spatial resolution and soft tissue contrast without use of potentially harmful ionizing radiation or radiotracers. MRI works as a result of the magnetic moment alignment of protons within a sample on application of a large external MF. In the case of MRI using SPIONs, coupling of their magnetic moment with those of nearby protons causes spin dephasing and the proton relaxation time shortening. To improve the sensitivity of MR signals from the background, various T1-W and T2-W contrast agents are continuously being developed. T1-W contrast NPs based on Fe, Gd and Mn are apt for documenting morphological information, while T2-W contrast is applicable for edema and inflammation detection, where IONPs are often employed [118–121]. The United States Food and Drug Administration (FDA) in December 1996, approved GastroMARK (AMAG Pharmaceuticals), an aqueous suspension MRI contrast medium of silicone coated, SPIONs, for oral administration for enhanced delineation of the bowel from adjacent organs and tissues. The approval of SPIONs based GastroMARK was considered a landmark moment in clinical nanomedicine that spurred research interest in this field [122]. Consequently, a slew of novel SPION-derivatives were developed, few were approved by the FDA and the European Commission (EC) as well for clinical use. On the other hand, the clinical trials employing SPIONs considerably increased, broadening their prospective biomedical applications. However, 16 years on, only GastroMARK and ferumoxytol are available commercially. Ferumoxytol are ultra-small SPIONs (USPIONs),

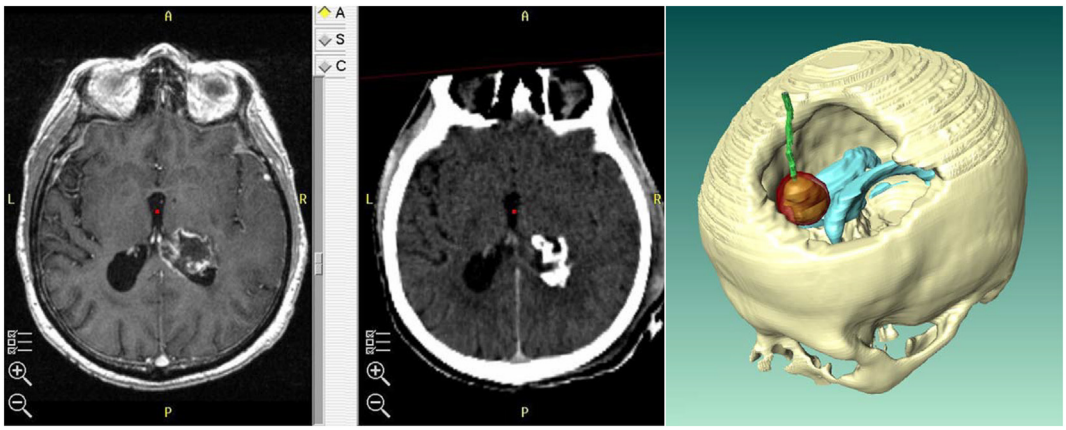

Fig. 4. Preoperative MRI with glioblastoma multiforme infiltrating the right posterior horn of the ventricle (left). The postoperative CT shows the MNPs as hyperdense areas within the tumor tissue (right). Three-dimensional reconstruction (MagForce NanoPlan software) of a skull with a frontal GBM after MRI and CT. Calculated 42 °C treatment isotherm surface (transparently red) enclosing the whole tumor (brown), thermometry catheter (green), ventricle (light blue). Reproduced with permission [115].

(~17–31 nm), coated with polyglucose sorbitol carboxymethylether [123]. Early clinical trials, demonstrated the superiority of ferumoxytol over traditional I.V. iron treatments, which had several safety concerns including inadequate dosage and systemic side effects, that were overcome with improved pharmacokinetics and facile administration modes. Another application of Ferumoxytol in several clinical trials is for imaging of diseases, ranging from multiple sclerosis to various cancers (e.g. prostate, bladder, breast, lung, ovarian, etc.) to heart conditions and type 1 diabetes [124]. In one of the study, a commonly used MRI contrast agent gadoteridol is directly compared with ferumoxytol, in a patient with GBM [125]. Gadoteridol agents are connected to nephrogenic systemic fibrosis, thereby limiting its use in patients with low glomerular filtration rates. Ferumoxytol, is projected as an attractive candidate to address this issue. T1-W and T2-W images of a patient's brain tumor for gadoteridol (background precontrast) and ferumoxytol (24-hour lag) were recorded and was found that ferumoxytol enhanced contrast in areas where gadoteridol could not. This enrichment of contrast was attributed to the presence of inflammatory cells, as ferumoxytol is a NP and is engulfed by macrophages. In 2003, Harisinghani et al. documented high-resolution MRI in patients with prostate cancer using IONPs where small and otherwise undetectable lymph-node metastases could be monitored, projecting the excellent sensitivity and specificity of the technique [126]. These results and the like prompted an increase in the number of clinical trials using IONP-enhanced MRI for the detection of sentinel lymph nodes in prostate cancer, with bladder, breast, and renal cancers, among others also being investigated (see Table 2). Clinically, Gd-chelates are the frequently employed I.V. T1-W MRI contrast agents owing to their high contrast and biocompatibility. For instance, a Gd-based T1-W MRI contrast media with high realxivity value (21.89 $mM^{-1}s^{-}1$) was synthesized by Chen et al. This value is significantly higher to that of Omniscan (4.64 mM^{-1} s^{-1}), a commercially available agent, demonstrating the former's broad prospect for clinical application [127]. Lin et al. developed complexes based on Gd (MSN-Gd) for better performance in MRI guided imaging and therapy [128]. Mn-based complexes have also been studied for T1 contrast ability as they display excellent paramagnetism, commendable contrast and better biocompatibility than Gd complexes. Significantly enhanced T1-W MR signals and long tumor persistence time were obtained with Mn metalloporphyrins such as all-round porphyrin dyad NPs (TPD NPs) with inner metal free porphyrin (PS) and exterior Mn-porphyrin (T1 MRI contrast agent), which was responsible for the signal enrichment in tumor, and additionally facilitated uptake of NPs by tumor cells, thus resulting in good MRI contrast. Similarly, T2-W MRI has also been widely practiced with SPIONs as the preferred contrast media [129]. Another example is of RGD modified Fe_3O_4 NPs (2.7 nm), with relatively high r1 relaxivity ($r1 = 1.4\ mM^{-1}s^{-1}$) for tumor MRI [130]. SPIONs have generally been a negative contrast enhancement agent, by darkening T2-W images, but could be tailored for positive contrast enhancement in T1-W scans as well, conventionally provided by relatively toxic Gd chelates. For example, a SPION formulation exhibited twofold T1 contrast improvement as against commercial Gd-based clinical standard [131]. Further, deimmunized mouse monoclonal antibody (muJ591) were conjugated to SPIONs to specifically target a prostate biomarker for tumor targeted diagnostic agent [132]. Despite several advantages discussed herewith, MRI suffers from delayed imaging rate, weak accuracy and sensitivity, along with systemic toxicity of few commonly used contrast media. More attention and efforts are required to fashion safer and improved MRI contrast agents for biomedical applications.

4.3. Magnetic guided drug delivery

IONPs have been recently employed as nanocarriers for various bioactive molecules, some even under clinical settings. Several prominent chemotherapeutics have been delivered by SPIONs to cancer tissue [133]. Liu et al. designed a magnetically controlled drug release system composed of a collapsible iron oxide core immersed in a H_2O-vitamin B12 solution and a fast-breathing nanosized two-layer shell of thermolabile polymer (PEO-PPO-PEO), and a stabilizing cross-linked outer shell. An externally magnetic field heated the nanocapsule causing volume change and eventually, disruption of outer shell will effectuate drug release. On exposure to high frequency AMF (HAMF), heat is generated in the superparamagnetic cores of nanocarriers which boosts drug release, a phenomenon termed as the MHT effect [134]. Once again, DOX (hydrophillic) and IONPs were encapsulated in a poly (vinyl alcohol) (PVA) coat, with hydrophobic PTX. Switching ON and OFF a 50 kHz external magnetic field, regulated the release rate of both drugs which increased (ON) and decreased (OFF), respectively, showcasing the potential of SPIONs as on-demand drug release modulators by merely regulating the AMF intensity and duration [135]. In another study, DOX was conjugated to MNPs (fluidMAG-CMX) and under an OMF the magnetically triggered release studies were performed. Significantly higher DOX release (70%) was recorded under the OMF. Additionally, in vivo experiments revealed that the tumor-curbing efficiency of CMX–DOX NPs was significantly higher under a magnetic field, than controls [136]. In a different setting, magnetic polymerosomes loaded with DOX was shown to exhibit regulated drug release under RF magnetic stimuli, leading to dual therapy: chemo as well magnetic hyperthermia. The HT effect of USPIOs was at work here, inducing polymersomes' membrane permeability, which melts the semicrystalline polycarbonate block leading to controlled drug release pattern [137].

5. Ultrasound responsive theranostics

In US imaging, which is an established clinical medical imaging tool, the image is created by tissue-reflected US waves which have density difference from the surrounding medium. However, a major issue is the compressibility of vasculature or other blood containing tissues due to which the obtained contrast may not be obvious enough, the reason why contrast enhancement agents are indispensable. US, as with the other modes of imaging discussed so far, is also non-invasive, and allows for spatiotemporal control with millimeter precision [138–140]. Apart from imaging, a focused US beam can induce drug release via localized heating due to the accumulation of acoustic energy at the focused region [141]. To overcome the inferior image resolution of US as compared to MRI or X-ray CT, US imaging contrast agents (UCAs) are widely employed in clinical examinations. UCAs are acoustically active to externally applied US energy, thereby amplifying echo signals and in turn enhancing image resolution based on differential echogenicity [142]. The larger acoustic impedance difference between solid phase and soft tissues implies that compared to softer UCAs, inorganic NPs with rigid structure can provide better US imaging resolution. Shklyar et al. emphasized that the aggregates of nano metal oxides (Al_2O_3, Fe_xO_y and ZrO_2) in aqueous media could efficiently contribute to the US image brightness, though theoretically, individual NPs (~50 nm) seem acoustically inactive, which implied that the acoustic signal intensity and aggregation degree were directly correlated. These observations have inspired a new aggregation-modulated image intensification mechanism, wherein target cells are treated with large NP aggregates, for real-time US imaging [143]. Among the varied inorganic nanomaterial UCAs, SiNPs due to their low toxicity, low hemolytic activity and relatively higher biodegradability have found special attention and FDA approval as well. Chiriaco et al. studied Si nanospheres for enhancing US imaging utilizing conventional diagnostic frequencies (7.5 to 10 MHz), with an emphasis on the size-effect of SiNPs on US imaging backscatter. It was determined that <50 nm NPs at lower concentrations could hardly be detected; whereas, prominent peaks of US backscattering were recorded with ~330 nm NP aggregates at relatively higher frequencies (3.5 and 4.5 MHz) [144]. Jokerst et al. developed a 300 nm SiNPs based tri-modal imaging (fluorescent, MRI and US) system for stem cells. It was revealed that intracellular SiNPs aggregation amplified the US backscattering by a magnitude seven times higher as compared to controls [145]. Foroutan et al. constructed biodegradable P_2O_5-CaO-Na_2O glass nanosphere (PGN)-based UCAs. These PGNs, owing to their phosphate-based composition and glassy nature, exhibited superior biodegradability than pure Si-based UCAs. Results showed

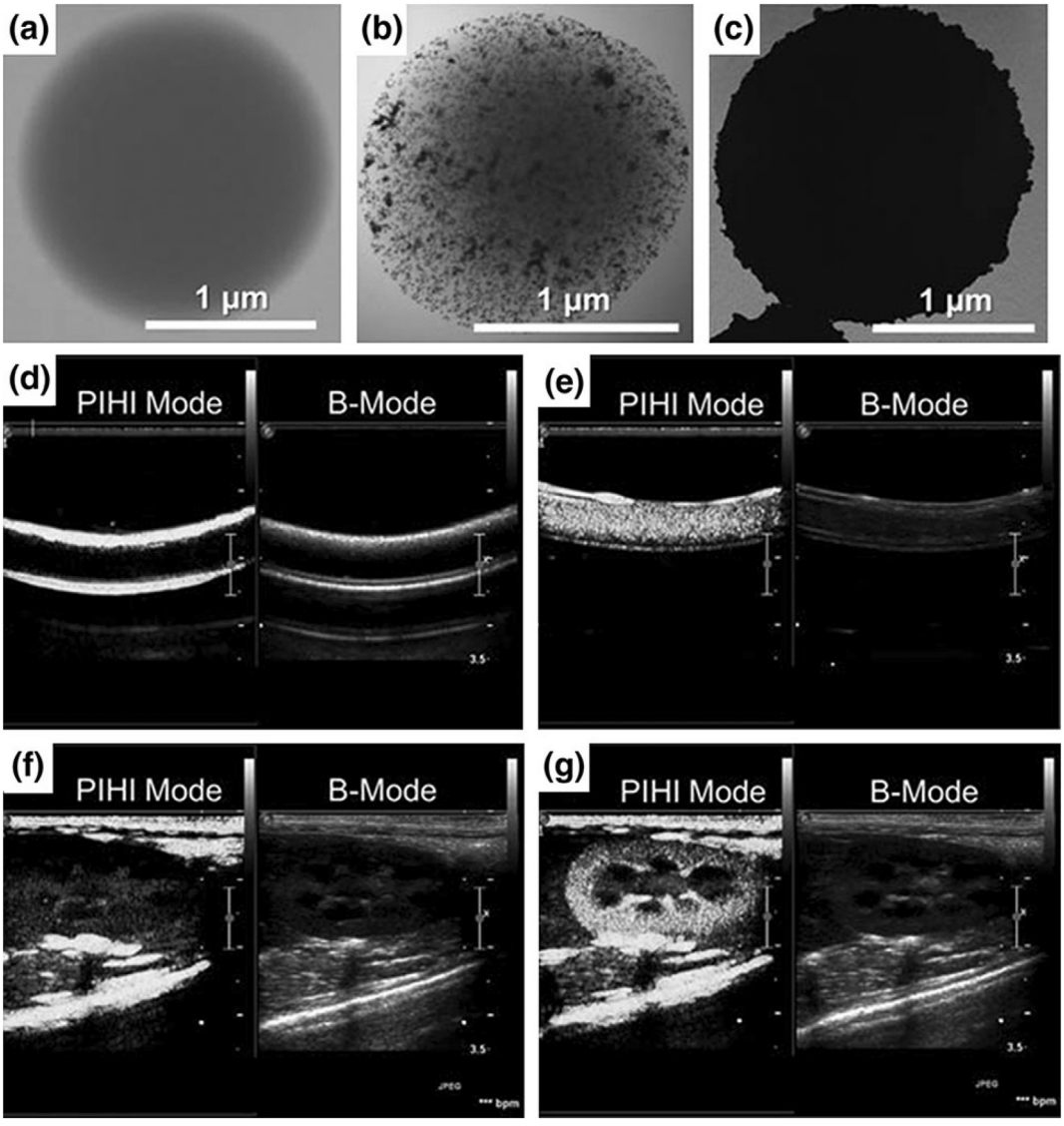

Fig. 5. TEM images of GNMs at different stages of the fabrication route; in vitro US contrast images of control (d) and GNMs (e) in a latex tube, in vivo US contrast images in the rabbit right kidney before (f) and after (g) administration of GNMs. Reproduced with permission [152].

persistent PGN-US signals for 4 h post-immersion in a standard phosphate buffered saline (PBS) solution, underlining its continuous US imaging capability [146]. Zhang et al. designed rattle-type SiNPs to elucidate the 'multi-scattering/reflection' concept. The structure's acoustic property was evaluated against solid and hollow SiNPs with rattle structure's linear scattering contribution (ISC) to be 44 % and 47 % higher than other structures, respectively. Also, a 39 % increase in reflection contribution percentage (IRC) was recorded for rattle structure when compared to other types. These rattle-type SiNPs demonstrated efficient US imaging in VX2 solid liver tumor model. The results describe the multilayer design to efficiently boost the US imaging quality in line with the 'multi-scattering/reflection' concept [147]. Gas-generating inorganic NPs are being increasingly explored with respect to applications in US imaging. For example, commercially available Prussian blue NPs (PBNPs) were developed by Yang et al. for US guided-detection of inflammatory regions, as the hydrogen peroxide (H_2O_2) in the inflammatory region could, by a chemical catalytic process, produce O_2 microbubbles (MBs) in the presence of PBNPs. A mean gray scale of US image had 80 % enhancement in 15 min of PBNPs injection in an in vivo inflammatory model, which could determine quantitative evaluation of inflammatory degree [148]. Similarly, another O_2 generating nanosystem is manganese dioxide (MnO_2). Gordijo et al. affirmed that polyelectrolyte-coated (PMD) MnO_2 NPs could generate O_2 on reaction with H_2O_2. Though the advantage of MnO_2 NPs against hypoxic tumor was described, additionally, this O_2 generation property of MnO_2 NPs can be extended to US contrast imaging as well [149]. Min et al. formulated DOX-loaded calcium mineralized NPs (DOX-$CaCO_3$-MNPs) for application in US imaging. Strong US backscattering was achieved from this inorganic nanosystem, due to CO_2 MBs production in acidic environment of tumors. The integrated PA and US imaging fuses pros of both techniques, with US imaging providing morphological details while, PA imaging offers more functional aspects about hemoglobin and O_2 saturation. Therefore, conferring functions of PAI to conventional UCAs, a bimodal contrast agent is fabricated, with advantages of both techniques while overcoming individual limitations [150]. Au NRs are the most widely investigated PAI agents due to their higher NIR absorption efficiency and PCE. Recently, much interest has been shown on the AuNR-incorporated UCAs. Wang et al. designed PA/US CAs by comprising albumin shelled MBs encapsulated with cystamine surface-modified AuNRs (AuMBs). The resultant AuMBs had significant effects in both US and PA (760 nm excitation). Additionally, the cystamine on AuNRs could be utilized for antibody modification for targeted delivery as well [151]. Ke et al. developed a Au-nanoshell-microcapsule (GNM) exhibiting a wide absorption range (650 and 900 nm), apt for NIR-PTT. Meanwhile, GNM assisted remarkable brightness enrichment of image in pulse-inversed harmonic imaging (PIHI) could be seen in

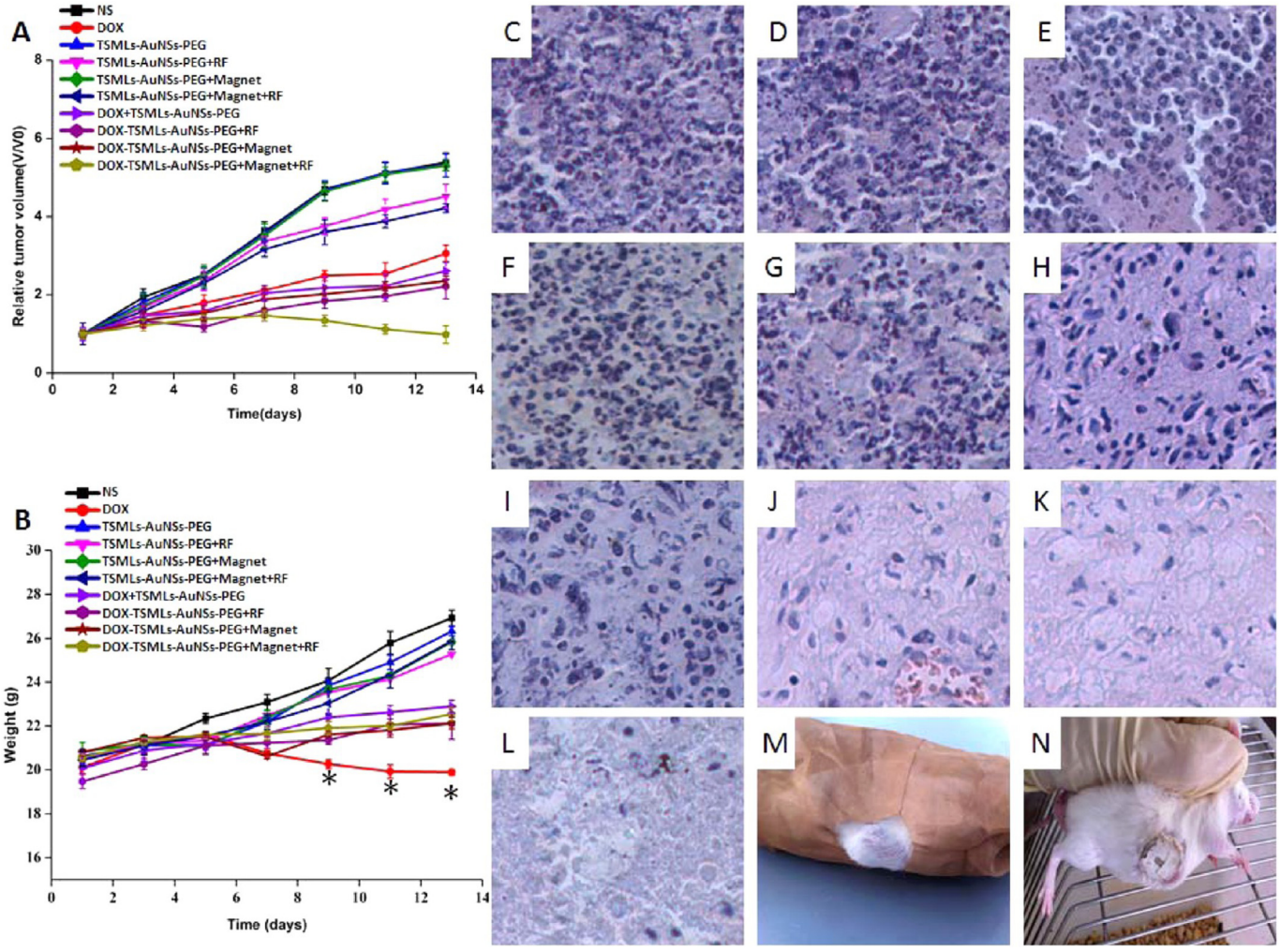

Fig. 6. MR images of (A) control and (B) DOX-TSMLs-AuNSs-PEG in vivo. X-ray images of (C) control (31 HU) and (D) DOX-TSMLs-AuNSs-PEG (185 HU) in vivo (4 h after injection). (A) Changes of relative tumor volume and (B) body weight of tumor-bearing mice in different groups during treatment (Mean ± SD, n = 6). Histologic assessments of tumor tissues with H&E staining (400 ×): (C) NS, (D) TSMLs-AuNSs-PEG, (E) TSMLs-AuNSs-PEG+RF, (F) TSMLs-AuNSs-PEG+Magnet, (G) TSMLs-AuNSs-PEG+Magnet+RF, (H) DOX, (I) DOX TSMLs-AuNSs-PEG, (J) DOX-TSMLs-AuNSs-PEG+RF, (K) DOX-TSMLs-AuNSs-PEG+Magnet, and (L) DOX-TSMLs-AuNSs-PEG+Magnet+RF. Photos of (M) tumor-bearing mice after irradiation with RF (mice were wrapped with copper net, and the tumor sites were uncovered) and (N) tumor-bearing mice treated with a magnet. Reproduced with permission [159].

latex tubes. On the other hand, within few seconds of GNM I.V. injection, significant enhancement in image of rabbit kidney was observed, confirming the excellent contrast enhancement ability of the GNMs in US imaging, with additional dual function as imaging-guided PTT (Fig. 5) [152]. Similarly, an on-demand drug release system of Au Nanocages (AuNcg), based on high-intensity focused ultrasound (HIFU) was developed, where the hollow AuNcgs were filled with 1-tetradecanol (PCM) with a melting point of 38-39 °C. On direct heating or HIFU, PCM quickly melts and escapes, along with encapsulated molecules (dye), from the AuNcgs interior into surrounding medium. It was concluded that the dye release from AuNcgs can be regulated by controlled the temperature or HIFU power. Meanwhile, when thermo-responsive pNIPAAm surface functionalized AuNcgs were exposed to HIFU, the polymer chains collapsed as temperature increased beyond the LCST, resulting in drug release. Switching off the HIFU, caused relaxation of the polymer chains back to their extended state, stopping the release, once again highlighting the on-demand features of these techniques. Also, as HIFU is deep tissue penetrative, this system can be used for monitored release at depths of up to 30 mm [153].

6. Radiofrequency Responsive Theranostics

Longer wavelength RF (10 kHz to 900 MHz) can also be explored for cancer cell ablation by the HT effect. RF has superior tissue penetration than NIR light, enabling treatment of deep seated tumors [154]. Interestingly, RF ablation for hepatic carcinoma therapy has already recieved FDA approval. However, current RF ablation faces many limitations as non-specific and invasive heating etc. a reason why nanomaterials are being explored for the enhancement of RF ablation cancer therapy [155]. Raoof et al., post cellular internalization of antibody-conjugated AuNPs (AuNPs), exposed them to an external RF field, resulting in the absorption of RF by AuNPs and dissipation of heat energy to kill cancer cells [156]. SWNTs have also been found to enhance RF ablation therapy, which was explained by Curley et. al. in 2007 [157]. Another study by Elsherbini et al. employed Au-coated magnetic for dual-mode HT, by laser and RF irradiation against subcutaneous Ehrlich carcinoma in mice. Analysis of results revealed more than 50% of the tumors disappeared completely on light/RF irradiation [158]. Wang and co-workers deployed Au coated magneto-liposomes for multiple actions as RF triggered release, chemo-HT, as well as MRI and X-ray CT (Fig. 6). These nanocomposites showed potential as drug delivery vehicles and effective imaging agents [159]. Though X-ray induced ionizing radiation and RF triggered HT combined with imaging modalities are examples of remotely triggered treatments with potential in theranostics platforms, the nanomaterials based RF ablation therapy is not yet fully deciphered, requiring extensive research and trials.

7. Radiation Responsive Theranostics

Positron Emission Tomography (PET) is an imaging modality in the field of nuclear medicine, providing real-time 3-D images of biological functional progress. Detection of pairs of γ rays emitted from a tracer (positron-emitting radionuclide) in conjugation with biologically active molecule can be utilized to develop 3-D images. Superior sensitivity and less background noise warrants PET as an excellent tool for biodistribution and pharmacokinetic studies. Radioisotopes ^{11}C, ^{18}F and

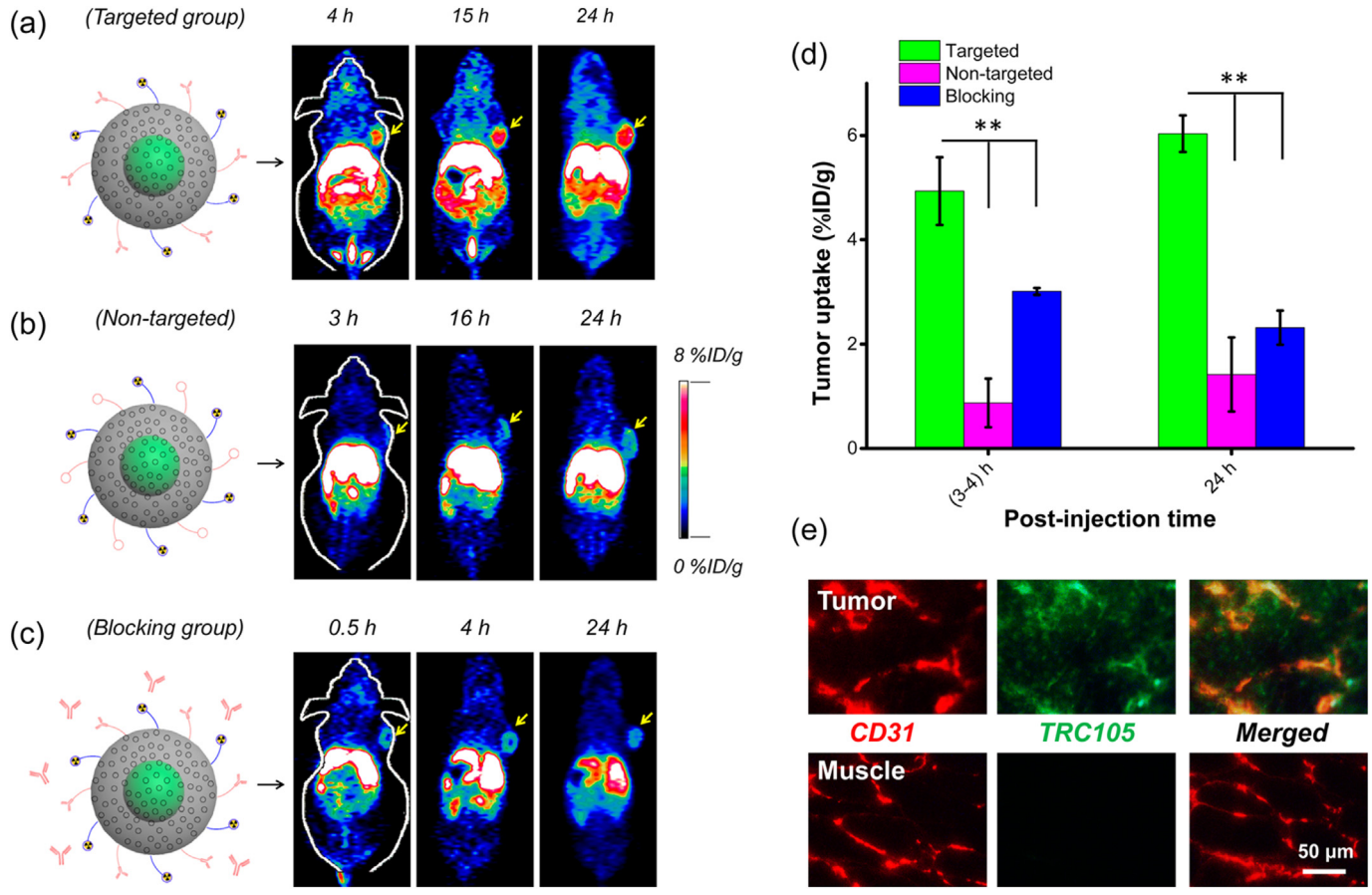

Fig. 7. In vivo CD105 targeted PET imaging, tumor uptake comparison and histology studies. In vivo serial coronal PET images of ^{64}Cu-CuS@MSN-TRC105 nanoconjugates (a, targeted group), ^{64}Cu-CuS@MSN (b, nontargeted group) and ^{64}Cu-CuS@MSN-TRC105 with a large dose of free TRC105 (c, blocking group) in 4T1 murine breast tumor-bearing mice at different time points postinjection. (d) Tumor uptake comparison among 3 different groups. The difference between 4T1 tumor uptake in targeted group and two control groups were statistically significant (**$P < 0.01$). (e) Ex vivo histology analysis of the tumor tissue slices with CD31 (red, with antimouse CD31 primary antibody) and CD105 (green, using the TRC105 from ^{64}Cu-CuS@MSN-TRC105 as the primary antibody). Muscle slices were also provided. Tumors were marked with yellow arrows. Reproduced with permission [163].

Table 1
List of few external stimuli responsive multifunctional nanoparticles in cancer theranostics.

Nanoparticle	Therapeutic	Diagnostic	Cancer	Pre-clinical(PC)/In vitro (IV)	Ref
Carbon-based					
Carbon Dots	PTT	FI, PA	HeLa	PC	[184]
Graphene QD	PDT	FI	MDA MB-231	PC	[185]
Graphene	PTT	FI	4T1	PC	[186]
CNTs	PTT	-	KB	PC	[187]
SWCNT	PTT	FI, MRI, Raman	4T1	PC	[188]
Carbon Nanotubes	PTT	FI	4T1	PC	[189]
ICG-Graphene Oxide	PTT	-	KB	PC	[190]
Dox-Graphene Oxide-Gd complex	Ch	MRI	HepG2	IV	[191]
Methylene blue-Graphene Oxide	PTT, PDT	-	HeLa	PC	[192]
Gold-based					
Gold Nanostar	PTT	CT, TPL, SERS	Sarcoma	PC	[193]
Gold Nanovesicles	PTT	PA	MDA MB-435	PC	[194]
Gold Nanorod-Photosensitizer	PDT, PTT	FI	SCC7	PC	[195]
Gold Nanoshell Micelle	PTT, LT-Ch	MRI	HeLa	IV	[86]
Gold shell-radiolabeled core nanoballs	-	PET, CT, CLI	4T1	PC	[196]
Gold Nanorods	PTT	PET, PA	U87MG	PC	[104]
Gold core with RAMAN tag	-	MRI, PA, Raman	U87MG	PC	[105]
Gold Nanoparticles	Ch	FI-DF	MCF-7	IV	[197]
Gold Nanomicelles	PTT, Ch	CT	MCF-7	PC	[198]
Gold Bellflowers	PTT	PA	4T1	PC	[199]
Au NPs	PTT, Ch	-	GI-1	IV	[200]
Ce6 Loaded Gold Vesicles	PTT, PDT	FI	MDA MB-435	PC	[201]
Copper based					
^{64}Cu-CuS Nanoparticles	PTT	PET, CT	U87	PC	[202]
Co_9Se_8 Nanoplates	PTT, Ch	PA, MRI	HepG2	PC	[203]
CuS Nanoparticles	-	PA	-	PC	[204]
CuS Nanocrystals	PTT	PET, CT	4T1	PC	[205]
CuS@MSN	PTT	PET	4T1	PC	[163]
$Cu_{2-x}Se$ Nanoparticles	PTT, LT-Ch, PDT	-	MCF-7	PC	[206]
Polymer-Microsphere-Encapsulated CuS Nanoparticles	PTT, Ch	MRI	4T1	PC	[207]
Dox-CuS Nanocrystals	PTT, Ch	-	4T1	PC	[208]
CuS Nanodots	PTT	PA, MRI	4T1	PC	[209]
Cu_5FeS_4 Nanoparticles	PTT	MRI, PA	4T1	PC	[210]
Copper Bismuth Sulfide Nanoparticles	PTT, PDT	CT	MCF-7	PC	[211]
CuS nanodots (CuSNDs) on doxorubicin ladened mesoporous silica nanoparticles	PTT	PA, PET	MDA MB-231, HepG2	PC	[212]
Cu_2S NCs	PTT, Ch, LT-Ch	PA, CT, FI	GI-1	IV	[213]
Copper sulfide doped periodic mesoporous organosilica nanoparticles (CuS@PMOs) loaded with DOX	PTT, LT-Ch	FI	U87MG	PC	[214]
CuS Nanotriangles	-	PA, MRI	U87	PC	[215]
Cu_2Te	PTT, Ch	CT, PA	MDA-MB 435	IV	[216]
^{64}CuS nanoparticles	-	PET	Melanoma	PC	[217]
Cu_9S_5 Nanocrystals	PTT	-	PC3	PC	[218]
Hollow Mesoporous Cu_2S	PTT, Ch, LT-Ph	FI	MCF-7	PC	[219]
Other nanomaterials					
MoS_2 Nanosheets	PTT, LT-Ch	CT	PANC-1	PC	[46]
Mo_{154}-core Nanocomposite	PTT, Ch	-	4T1	PC	[220]
MoS_2 Nanoflakes	PTT	-	4T1	PC	[221]
MoS_2	PTT	-	HeLa	IV	[222]
MoS_2 Nanoflakes	PTT	-	4T1	PC	[223]
UC Nanophosphor	-	UCLu, MRI	-	PC	[224]
UCNPs	PDT	UCLu	LLC	PC	[225]
UCNPs	PTT	UCLu	HeLa	PC	[226]
WS_2 Nanosheets	PTT	CT, PA	4T1	PC	[227]
TiS_2 Nanosheets	PTT	PA	4T1	PC	[228]
Doxorubicin Loaded Magnetic Polymersomes	Ch, MT-Ch, MHT	MRI	-	-	[137]
Hollow structured polymer–silica nanohybrid	PTT, Ch	-	S180	PC	[229]
Bi_2S_3 Nano-urchins	PTT	CT, PA	HeLa	PC	[230]
Bi_2S_3-embedded mesoporous silica nanoparticles	RT, Ch	-	PC3	PC	[176]
Bismuth Sulfide	PTT	MSOT, CT	4T1	PC	[231]
Ag Nanodots	PTT	CT	4T1	PC	[232]
Ag_2S Nanodots	PTT	FI, PA	4T1	PC	[233]
Hybrid nanomaterials					
MoS_2/Bi_2S_3	PTT, RT	CT, PA	4T1	PC	[234]
GdOF:Ln@SiO_2-ZnPc	PTT	UCL, CT, MRI	H22	PC	[235]
Cy5.5-HANP/CuS Nanoparticle	PTT	FI, PA	SCC7 tumor	PC	[106]
Graphene oxide coated Gold Nanorods	PTT	PA	-	PC	[236]
^{64}Cu-Gold NPs	PTT	PET	U87MG	PC	[97]
MnSe@Bi_2Se_3	PTT, RT	CT, MRI	4T1	PC	[48]
Fe_3O_4 Core@hybrid@Au Shell	PTT	MRI	MCF-7	PC	[237]
Metal doped WS_2 Nanoflakes	PTT	PA, CT, MRI	4T1	PC	[238]

Table 1 (*continued*)

Nanoparticle	Therapeutic	Diagnostic	Cancer	Pre-clinical(PC)/In vitro (IV)	Ref
$Fe_3O4@Cu_{2-x}S$ Core−Shell	PTT	MRI	HeLa	PC	[239]
Lanthanide-Doped Nanoparticles	PDT	UCLu, MRI	U87MG	PC	[240]
Graphene- Magnetic Nanocomposite	PTT	MRI, CT	4T1	PC	[241]
^{131}Iodine-Doped Copper Sulfide Nanoparticles	PTT, RT	CT	4T1	PC	[242]
$Fe_3O_4@SiO_2$@gold nanorods@mesoporous SiO_2	PTT	MRI	KB	IV	[243]
Gold-Coated Fe_3O_4 Nanoroses	PTT, Ch	OI, MRI	CCL-119 T-cell, Ramos	IV	[244]
Graphene oxide-UCNP	PTT, PDT	Fl	-	PC	[245]
Iron Oxide Decorated MoS_2 Nanosheets	PTT	PET, PA, MRI	4T1	PC	[246]
Manganese (II) Chelate Functionalized Copper Sulfide Nanoparticles	PTT	MRI, PA	MDA MB-231	PC	[247]
MSN coated CNT	PTT, LT-Ch	PA, MRI	4T1	PC	[87]
Graphene Nanosheets-Magnetic NPs	PTT	Fl, MRI	4T1	PC	[248]
Noble metal coated SWCNT	PTT	SERS	KB	IV	[249]
(DOX)-loaded hollow mesoporous CuS nanoparticles (HMCuS NPs) with superparamagnetic iron oxide nanoparticles	PTT, Ch	MRI	MCF-7	PC	[250]
$CdSe/Cu_2S$	PTT	Fl, CT, PA	Gl-1	IV	[251]
QD-Reduced Graphene Oxide	PTT	Fl	MCF-7	IV	[252]
γFe_2O_3 @Au MagneticGold Nanoflowers	PTT	MRI, PA, SERS	4T1	PC	[253]
Fe_3O_4@CuS Nanoparticles	PTT	MRI	HeLa	PC	[254]
Graphene oxide loaded Gold Nanorod Vesicles	PTT, LT-Ch	PA, PET	U87MG	PC	[255]
MoS_2/Fe_3O_4	PTT	MRI, PA	PANC1	PC	[256]
$Au-Cu_9S_5$ Nanoparticles	PTT	CT	CT26	PC	[65]
$WS_2@Fe_3O_4$ nanocomposite with mesoporous silica coating	PTT, LT-Ch	Fl, MRI, CT	4T1	PC	[257]
Pt(IV) conjugated nano-graphene oxide	PTT, Ch	-	4T1	PC	[258]
Carbon Nanosphere with Patchy Gold	PTT	-	MCF-7	PC	[259]
Copper Sulfide Perfluorocarbon Nanodroplets	-	PA, US	-	PC	[260]
Core–Shell Pd@Au Nanoplates	PTT	PA, CT	4T1	PC	[261]
Fe_3O_4 /Ag Complexed Cores in Hollow Gold Nanoshells	PTT	MRI	Melanoma	PC	[262]
$Fe@Bi_2S_3$ Nanocomposites	PTT, RT	MRI, CT	4T1	PC	[263]
FeS Nanoplates	PTT	MRI	4T1	PC	[264]
Pt-UCNPs	LT-Ch,	UCLu, MRI, CT	H22	PC	[265]
$Cu–Ag_2S$ nanoparticles	PTT	PA	4T1	PC	[266]
CuInS/ZnS Quantum Dots	PDT	Fl, MSOT, PET	4T1	PC	[267]
Graphene Oxide Loaded with Gold Nanostars and Doxorubicin	PTT, Ch	-	4T1	PC	[268]
^{68}Ga-radiolabeled AGuIX nanoparticles	RT	PET, MRI	U87MG	PC	[269]
Gold-Silica Quantum Rattles	PTT	Fl, PA	LS174T	PC	[270]

PTT: Photothermal therapy; PDT: Photodynamic therapy; Ch: Chemotherapy; LT-Ch: Light Triggered Chemotherapy, MHT: Magnetic Hyperthermia; RT: Radiation therapy, MT-Ch: Magnetic Triggered Chemotherapy; PA: Photoacoustic imaging, MRI: Magnetic Resonance Imaging, CT: X-ray Contrast Imaging, Fl: Fluorescence, UCLu: Upconversion Luminescence, PET: Positron Emission Tomography, SERS: Surface Enhanced Raman Scattering, OI: Optical Imaging, TPL: Two Photon Luminescence, MSOT: Multispectral Optoacoustic Tomography

^{15}O (for drugs), heavy metal isotopes ^{64}Cu, ^{68}Ga, ^{99}Tc and 111 In (for antibodies/peptides), and functional molecules as DOTA (1,4,7,10-tetraazacyclclododecane-1,4,7,10-tetraacetic acid) and TETA (1,4,8,11-tetraazacyclotetradecane-1,4,8,11- tetraacetic acid) represent common PET agents [160]. ^{124}I labeled cRGDY silica nanomolecular particle tracer employing clinical trial pilot study is currently underway to analyze PET imaging of patients with malignant brain tumor and melanoma (NCT01266096) [161]. A PET active radioimmunoconjugate composed of a zirconium (Zr89) labelled colloidal human serum albumin (HSA) was developed. Post in vivo administration, the Zr89 nanocolloidal albumin travels the bloodstream into the lymphatic system. PET enables clear visualization of the lymph node draining pattern alongwith the lymph node status, including the sentinel lymph node (SLN), which is facilitated by the smaller particle size of nanocolloidal albumin (NCT02850783) [162]. Time-dependent uptake of CuS@MSN by 4T1 tumor was evaluated by Chen et al. employing PET, and was found to be 4.9% ID/g (4 h post-injection) peaking at 24 h post-injection (Fig. 7). Higher CuS@MSN-TRC uptake than CuS@MSN was revealed by serial PET scans, indicating the enhancement efficiency of TRC 105 [163]. Likewise, Rodriguez et al. developed theranostic radiopharmaceutical ^{66}Ga-DOTA-E(c(RGDfK)) 2 to assess distribution and pharmacokinetics by PET. On other hand, CT is a widely employed clinical imaging module known for its high resolution, deep tissue penetration, low cost, and informative post-processing [164]. Similarly Liu et al. tested tungsten-based nanomaterials, PEGylated WO_{3-x} NPs, for CT contrast and CT-guided PTT. The PEGylated WO_{3-x} NPs clearly delineated the tumor during CT imaging due to its strong X-ray absorption. Importantly, there was no evident collateral damage to normal tissues due to this CT agent but significant NIR-triggered tumor ablation was achieved, proposing its potential in CT-guided cancer therapy [165].

Radiation therapy (RT) is commonly used in clinical cancer treatment employing high-energy radiations such as X-rays and γ-rays. Though predominantly used for sarcoma therapy, RT is acceptable for other cancer types as well, as radiation causes direct damage to nuclear DNA, resulting in curb on cellular proliferation. Indirectly mitochondrial DNA and other cellular components may also be damaged by radiation, by generation of ROS. Prolonged survival has been reported by RT following surgical resection. However, the systemic side-effects due to continuous high dose X-ray exposure, and radiation-resistance are prominent drawbacks of RT. Metal NPs with strong photoelectric absorbance could particularly improve RT sensitivity, acting as radiation dose-enhancing agents. For instance, AuNPs could mediate radiosensitization due to the greater absorption and deposition of energy in surrounding tissues from Auger electrons, photoelectrons and characteristic X-rays [166,167]. The novel radio enhancer NBTXR3, developed by Nanobiotix, utilizes a high e^- density metal oxide (HfO_2) NP to boost RT efficacy without increasing dose to the surrounding tissue. Incorporation of such novel materials increases X-ray interactions resulting in a larger number of excited e^- generating more reactive radical species. NBTXR3 showed similar antitumor effects as with conventional RT in preclinical trials, and a good safety profile in humans as well as encouraging antitumor results (early clinical trials) [168]. Phase I clinical trials for NBTXR3 began in 2011 and have since reached phase II/III for soft tissue sarcoma treatment, due for completion soon

Table 2
List of external stimuli responsive multifunctional nanoparticles for cancer theranostics in clinical trials.

Commercial Name	Cancer Type	Function	Status	CTI	Ref
MAGNABLATE I: Magnetic NP	Prostate Cancer	Thermoablation; Retention and Maintenance	C	NCT02033447	[112]
	Glioblastoma	Efficacy and safety of thermoablation monotherapy and in combination with radiotherapy	R	DRKS00005476	[113]
Ferumoxytol: Iron Oxide NPs	Pediatric Brain Tumors	MRI – Tumor vasculature imaging in pediatric brain tumors	A	NCT00978562	[273]
	Malignant Brain Tumors	MRI-Imaging biomarkers of malignant brain tumors	A	NCT00103038	[274]
	Adult/Pedi Sarcomas	MRI of lymph node	WD	NCT01663090	[275]
	Brain Tumors	MRI of tumor & tumor vasculature	R	NCT03234309	[276]
	Malignant Brain Tumors	MRI of macrophages	R	NCT03179449	[277]
	Stage IIB-IIIC Esophageal Cancer	MRI of Lymph Nodes	R	NCT02857218	[278]
	Non-small Cell Lung Cancer & Brain Metastases	MRI- in predicting true vs pseudoprogression after stereotactic radiosurgery	R	NCT03325166	[279]
	Bone Sarcoma	MRI – Imaging bone sarcomas and osteomyelitis	R	NCT01336803	[280]
	Rectal Cancer	MRI of Lymph Nodes	R	NCT03280277	[281]
	Brain Tumors	MRI - Measure Tumor Associated Macrophages and to Predict Patient Response to Treatment	A	NCT01770353	[282]
	Primary/Metastatic Brain Tumor	MRI - Blood brain barrier permeability to ferumoxytol; evaluate tumor microvascularity; microscopic distribution of ferumoxytol particles in tissue removed from subjects undergoing surgery	R	NCT00659126	[283]
	Esophageal Cancer	MRI-To identify metastatic lymph nodes		NCT02689401	[284]
	Locally Advanced Head & Neck Squamous Cell Carcinoma	MRI for Primary and Nodal Tumor Imaging	A	NCT01895829	[285]
	Lymph Node Cancers	MRI to "see" cancerous lymph nodes on an MRI scan	A	NCT01815333	[286]
	Prostate, Bladder & Kidney Cancers	MRI-Detecting Lymph Node Metastases	R	NCT02141490	[287]
	Thyroid Cancer	MRI-Pre-Operative Nodal Staging	C	NCT01927887	[288]
	Esophageal Neoplasms	MRI- Improve Treatment Stratification of Patients	R	NCT02253602	[289]
	Pediatric Cancer	MRI- Comparison of sensitivity, specificity and accuracy	R	NCT01542879	[290]
	Glioblastoma	MRI- Steady State Blood Volume Maps	R	NCT02359097	[291]
	Glioblastoma	MRI-Assessing early response post therapy	C	NCT00660543	[292]
	Primary Prostate, Breast Cancer	MRI- Imaging of Lymph Nodes	C	NCT00087347	[293]
	Melanoma & Glioblastoma	MRI in Assessing Response to Pembrolizumab in Patients	R	NCT03347617	[294]
	Prostate Cancer	MRI for detection of lymph node involvement	C	NCT01296139	[295]
	Colorectal cancer	MRI for Detecting Lymph Node Metastases	WD	NCT01983371	[296]
	High Grade Glioma	MRI to quantitatively image brain tumor vascularity	T	NCT00769093	[297]
	Glioblastoma	MRI based targeted biopsies	C	NCT02466828	[298]
Ferumoxtran-10: Iron oxide NPs	Locally Advanced Cervical Cancer or high-risk Endometrial Cancer	MRI- Lymph Node Metastasis	A	NCT00416455	[299]
	Bladder, Genitourinary, Prostate Cancer	MRI to detect pelvic cancers	T	NCT00147238	[300]
	Rectal & Breast Cancer	MRI to detect lymph node metastases	R	NCT02751606	[301]
	Prostate Cancer	MRI-Lymph Node Imaging	R	NCT03223064	[302]
	Breast Cancer	MRI to identify metastases to axillary lymph nodes	C	NCT00107484	[303]
	Brain Neoplasms	MRI-To aid biopsies	T	NCT00659334	[304]
	Uterine, Cervix, Bladder, Prostatic Neoplasms	MRI to image pelvic lymph nodes	C	NCT00188695	[305]
SPION	Pancreatic Cancer	MRI for pre-operative cancer staging	C	NCT00920023	[306]
AuroLase: Auroshell	Head & Neck Cancer	PTT- Photothermal ablation of target lesions	C	NCT00848042	[52]
	Primary and/or Metastatic Lung Tumors	PTT- Photothermal ablation of target lesions	T	NCT01679470	[53]
	Neoplasms of Prostate	Focal ablation of lesion; MRI/US fusion imaging	R	NCT02680535	[58]
CYT-6091: TNF bound Colloidal Gold	Adult Solid Tumor	Tolerated dose study	C	NCT00356980	[50]
	Adrenocortical Carcinoma Breast Cancer Colorectal Cancer Gastrointestinal Cancer Kidney Cancer Liver Cancer Melanoma (Skin) Ovarian Cancer Pancreatic Cancer Sarcoma	To determine the tumor tissue and normal tissue distribution of colloidal gold-bound tumor necrosis factor in patients	C	NCT00436410	[307]
NANOM-FIM	Atherosclerosis	Plasmonic Nanophotothermal Therapy	C	NCT01270139	[59]
Cornell Dots: Silica nanoparticles with a NIR fluorophore, PEG coating, and a ^{124}I radiolabeled cRGDY targeting peptide.	Melanoma and Malignant Brain Tumors.	PET- To characterize biodistribution, pharmacokinetics, and metabolic stability	A	NCT01266096	[161]
	Head and Neck Melanoma, Gynecologic Malignancies, Breast Cancer	Real-Time Image-Guided Intraoperative Mapping of Nodal Metastases	R	NCT02106598	[308]
Sienna+: Sentimag	Breast Cancer	Identification of sentinel lymph node	U	NCT01790399	[309]
SENTINAC-01: Superparamagnetic Iron	Breast Cancer	Sentinel Lymph Node Biopsy in Patients with Node-Positive	U	NCT02249208	[310]

Table 2 (*continued*)

Commercial Name	Cancer Type	Function	Status	CTI	Ref
Oxide		Breast Cancer			
NBTXR3 Crystalline Nanoparticles: Hafnium	Soft Tissue Sarcoma	Radiation Therapy activated by external beam radiation	C	NCT01433068	[168]
Oxide	Locally Advanced Squamous Cell Carcinoma of the Oral Cavity or Oropharynx	Intensity Modulated Radiation Therapy	R	NCT01946867	[171]
	Soft Tissue Sarcoma	Radiation therapy	A	NCT02379845	[169]
	Liver Cancers	Radiation therapy	R	NCT02721056	[172]
	Head and Neck cancer	Radiation therapy with concurrent Chemotherapy	R	NCT02901483	[170]
	Rectal Cancer	Radiation and Chemotherapy	R	NCT02465593	[311]
	Prostate Adenocarcinoma	Radiation therapy	R	NCT02805894	[312]
AGuIX: Polysiloxane Gd-Chelate NP	Gynecologic Cancer	Chemoradiation	NYR	NCT03308604	[173]
	Colon Cancer	Sentinel Lymph Node Imaging	C	NCT02850783	[162]

C: Completed, NYR: Not Yet Recruiting, R: Recruiting, A: Active, U: Unknown, T: Terminated; WD: Withdrawn

[169]. Phase I trials for head and neck cancer have begun and have been completed for rectal cancer in conjunction with PharmaEngine under the name, PEP503 [170]. Another clinical trial currently recruiting, utilizing the same particles against advanced squamous cell carcinoma of the oral cavity or oropharynx [171]. NBTXR3 is also being investigated at Phase I/II to assess their safety and efficacy by intralesional (IL) or intraarterial (IA) injection, activated by stereotactic body RT for liver cancer treatment [172]. Another nanocomposite, AGuIX-NP (Polysiloxane Gd-Chelates based NPs) is now in phase I clinical trial for safety evaluation and escalating dose/radiation combination tolerability in patients with locally advanced cervical cancer (NCT03308604) [173]. Meanwhile, polyethylene glycosylation modified AuNPs (P-GNPs) have shown ~1.61-fold increase in γ-H2AX foci density when compared to RT alone with improved tumor regression and overall survival [174]. Separately, AuNPs/SPIONs-loaded polymeric micelles have also demonstrated excellent RT outcomes with a 90-day survival of 71% mice using the nanoformulation RT, while only 25% for RT-treated mice [175]. Bi-based NPs have also exhibited strong X-ray radiation induced photoelectric absorbance and are able to generate multiple short-range secondary e^-, thereby elevating X-ray deposition in tumor tissues and accelerating DNA damage. For instance, Bi_2S_3 NPs were coated with MSNs which resulted in significant tumor eradication on radiation exposure [176].

Zhang et al., used different sized PEGylated AuNPs to enhance RT. NPs of 12.1 nm and 27.3 nm size displayed high radiosensitivity, which could be used to enhance RT efficacy induced by γ-radiation [177]. Such enhancement can be supplemented with allied therapies (e.g. PTT) for better treatment outcomes, as demonstrated by Shi and co-workers with their CuS coated UCNPs [178]. In addition to the X-ray absorbing NPs enhanced RT, another exciting strategy, utilizing X-ray luminescent NPs for X-ray triggered PDT is available. Liu et al., synthesized LaF_3:Tb^{3+}–meso-tetra(4-carboxyphenyl) porphine (MTCP) NPs for X-ray induced PDT. Upon X-ray exposure, PS MTCP is activated by visible light emitted from X-ray luminescent NPs, and generate $^1O_2$ or ROS to induce PDT. Such a strategy could also be employed for deep tumor treatment as X-rays are deep tissue penetrative [179]. Shi group, synthesized core-shell Ce^{III}-doped $LiYF_4$@SiO_2@ZnO (SZNPs) for synergistic RT and ionizing-radiation induced PDT. The nanoscintillators would emit UV light, triggering e^--hole pairs in the ZnO shell, leading to toxic hydroxyl radicals generation. In vivo experiments revealed much better therapeutic efficacy while using the nanoconjugate when compared to simple X-ray induced RT [180]. CeF_3 NPs conjugated with the PS verteporfin were used for ROS generation upon 8 keV X-ray irradiation and results revealing similar $^1O_2$ molecules per cell as PDT [181]. Additional reports focusing on X-ray induced PSs exist, including one with hypericin (PS) encapsulated lanthanide micelles [182]. Wei and Zhang demonstrated a RT/PDT combinatorial strategy for cancer treatment named self-lighting PDT (SLPDT). Upon exposure to X-rays, scintillation luminescence from the NPs, would activate the PSs and $^1O_2$ generation causes cancer cells destruction. Combining conventional RT with PDT would allow for lower dose radiation requirement to realize the desired effects [183]. For patients with terminal cancer, RT could relieve the symptoms and prolong their lives to an extent. However, RT has many short and long-term side effects even causing loss of organ functions. Hopefully, with advancements in techniques as radiation wave knife (gamma knife radiosurgery), the tumors may be dealt with more accurately for better clinical outcome.

8. Conclusions: Challenges and Future Directions

Nanotheranostics has rapidly progressed over the past decade and diversified its approach by incorporating multifunctional, biocompatible and biodegradable, systems that encapsulate drugs and diagnostic agents. Applications of this remarkable technology include, but are not limited to chemo-, radio-, biologic-, immuno- or gene therapies, or various compatible combinations of these [7–14]. An account of some highly relevant externally triggered nanotheranostics for the regulation of cancer are presented in this review and few more multimodal theranostics are tabulated in Table 1. Considerable attention has been attracted by the external stimuli-responsive, remotely triggered theranostic agents. The most exciting aspect of these trigger responsive modules is the non-invasive control that can be exercised over them, resulting in on-demand therapy/diagnosis. These remotely triggered nanoconstructs would allow clinicians to diagnose, plan and initiate therapy, and finally evaluate treatment outcomes while monitoring the NPs' pharmacokinetics in real-time [21–23].

However lucrative, all nanosystems-smart, theranostic or otherwise, are challenged by numerous deterrents that determine their overall application and fate. It is well established that the physicochemical properties of NPs can tremendously impact their behavior and performance. Numerous challenges exist with the primary concerns being identification of the choice of stimuli for the particular application, to fabricate materials that are responsive to certain specific or multiple stimuli to address a particular or group of issues, followed by biocompatibility analysis, where the ideal material should be nonimmunogenic and biodegradable.

For instance, in the case of light-triggered materials, the wavelength of light plays a major role in deciding the application region, as only particular regions of the spectrum can be utilized for clinical use. This is due to the fact that the penetration depth of light is dependent on its wavelength, as most of the incident light is either absorbed or scattered by skin, soft tissues and blood. Therefore the wavelength of light directly correlates to the operational depth of the nanoconstructs which have to be precisely positioned at the appropriate depth for activation, which is a challenging task. Owing to these reasons, the UV region has a maximum penetration limit of only 10 mm, restricting the UV-based phototherapies to treatment of superficial tumors (e.g. melanoma) or such tumors accessible using endoscopy procedures (e.g. cancers of

throat, esophagus, stomach etc.), the latter also for treatment of smaller remnant tumors after a surgical resection of the major tumor mass [22]. Apart from the wavelength dependent penetration restrictions, light-based therapies are also governed by laser power density values. Increasing the laser power dose could increase the effectiveness of a material, however, it has been established that a laser power density beyond 1 W/cm^2 is significantly harmful to biological systems. These hurdles can be overcome to a great extent when using materials that respond to higher wavelength light, such as NIR which exhibit less absorption/scattering by body tissues accompanied by much deeper penetration abilities (~1 cm) and minimal photo-toxicity. Apart from this, two-photon technology can be readily applied for converting the UV light source to NIR region [271]. Certain light-triggered nanosystems have an additional issue of low PCE, which directly translates in weak response like blinking luminescene, diminished signal intensities, poor thermal or ROS generation resulting in poor therapeutic outcomes etc.

Unlike light-triggered therapies, MF is not limited by penetration depth, with both MHT and magnetic tumor targeting entering clinical trials, while imaging techniques as MRI is already well established. Still, in order to effectuate sufficient heat generation for MHT, high concentrations of magnetic nanoparticles are injected directly into the tumor [22]. Also, issues related to degradation of noble-metal contrast agents in MF-dependent imaging, not only decrease the image quality but also pose critical toxicity issues and are partially responsible for increasing the operational costs [271]. Therefore, stable nanomaterials which respond to MF in a more efficient manner, without significant degradation and higher heat generation at relatively less concentrations with abilities to be manipulated towards tumors via systemic administration are required. Additionally, development of instrumentation capable of generating enhanced and precisely controlled MF would greatly augment the nanomaterial-based MF applications. Other issues related to MHT may be the AMF tuning which should be complementary to the responsive material or vice versa, any adverse change to this scenario would result in poor heating or overall magnetic response.

In the case of radiation therapies, the major issue still remains the radiation burden, as none of the radiation are specific to tumors alone and inadvertently cause critical damage to organs and tissues adjacent to the tumor or those in the path of irradiation. One solution could be the targeted delivery of the corresponding responsive nanomaterial to the desired area of irradiation, which are expected to minimize the off-site effects considerably, while developing nanomaterials requiring lower radiation dose for activation remains priority.

Ultrasound based applications are currently in use worldwide for various biomedical conditions mainly for deep tissue imaging. The introduction of US-responsive inorganic nanomaterials is expected to significantly enhance the application potential of US to not only diagnostic but theranostics as well. Knowledge of spatial and temporal characteristics is essential for developing novel nanomaterials which would efficiently work as US-responsive theranostic candidates [271].

Apart from the issues with treatment methods, the unpredictable behavior of nanomaterials promoted from the in vivo to clinical trial scenario with regards to exposure to the human body (i.e. biodistribution, toxicity, and degradation) remains elusive. Although a nanomaterial may have been proven safe and effective in multiple in vivo cases, the same may not be necessarily emulated in clinical trials. This is the primary reason why numerous prospective nanomedicine candidates get rejected at the early clinical stages whereas still many fail even after reaching III/IV level trial stages. One major concern is the complexity of tumor tissues, which differs vastly from in vivo experimental animal models to the human body, especially when considering EPR dependent nanomaterial administration. Active tumor targeting by specific ligands or exogenous stimulus could prove to be a viable solution, with the latter predicted to assist in more precise nanomaterial delivery, minimizing or completely eliminating premature leakage of drugs during blood circulation [272].

These are a few imminent issues that need to be addressed for the externally triggered nanotheranostic candidates, especially for inorganic nanomaterials, to be employed in clinical scenario. To summarize, choosing the appropriate external stimuli for the specific investigation is of prime importance. Further, designing biocompatible materials, targeted more or less precisely to the site of ailment/interest, and responsive to the respective stimulus at low doses and acceptable concentrations to elicit maximum effects is extremely crucial. Valuable lessons should be learnt from the failure/success of other researchers so as to implement and improve the positive aspects and steer clear of or modify the negative ones. Though few inorganic external stimuli responsive nanotheranostics have already passed pre-clinical stage and reached clinical trials (tabulated in Table 2), further investigations and testing is essential so as to cement the safety and efficacy profile of these nanotheranostic materials which definitely have the potential to revolutionize the way medical care is provided by giving an all new exciting dimension to it.

Reference

[1] W. Du, O. Elemento, Cancer systems biology: Embracing complexity to develop better anticancer therapeutic strategies, Oncogene. (2015)https://doi.org/10.1038/onc.2014.291.
[2] D. Hanahan, R.A. Weinberg, Hallmarks of cancer: The next generation, Cell. (2011) https://doi.org/10.1016/j.cell.2011.02.013.
[3] C.E. Meacham, S.J. Morrison, Tumour eterogeneity and cancer cell plasticity, Nature. (2013)https://doi.org/10.1038/nature12624.
[4] G.I. Evan, K.H. Vousden, Proliferation, cell cycle and apoptosis in cancer, Nature. (2001)https://doi.org/10.1038/35077213.
[5] M. Shackleton, E. Quintana, E.R. Fearon, S.J. Morrison, Heterogeneity in cancer: cancer Stem cells versus clonal evolution, Cell. (2009)https://doi.org/10.1016/j.cell.2009.08.017.
[6] R.A. Burrell, N. McGranahan, J. Bartek, C. Swanton, The causes and consequences of genetic heterogeneity in cancer evolution, Nature. (2013)https://doi.org/10.1038/nature12625.
[7] M.M. Amiji, Nanotechnology for cancer therapy, Curr. Mol. Med. (2010)https://doi.org/10.1201/9781420006636.
[8] T. Lammers, F. Kiessling, W.E. Hennink, G. Storm, Drug targeting to tumors: Principles, pitfalls and (pre-) clinical progress, J. Control. Release. (2012)https://doi.org/10.1016/j.jconrel.2011.09.063.
[9] G.A. Hughes, Nanostructure-mediated drug delivery, Nanomedicine Nanotechnology, Biol. Med. (2005)https://doi.org/10.1016/j.nano.2004.11.009.
[10] C. Wang, H. Xu, C. Liang, Y. Liu, Z. Li, G. Yang, L. Cheng, Y. Li, Z. Liu, Iron oxide @ polypyrrole nanoparticles as a multifunctional drug carrier for remotely controlled cancer therapy with synergistic antitumor effect, ACS Nano (2013)https://doi.org/10.1021/nn4017179.
[11] R. Bazak, M. Houri, S. El Achy, S. Kamel, T. Refaat, Cancer active targeting by nanoparticles: a comprehensive review of literature, J. Cancer Res. Clin. Oncol. (2015) https://doi.org/10.1007/s00432-014-1767-3.
[12] F.M. Kievit, M. Zhang, Cancer nanotheranostics: Improving imaging and therapy by targeted delivery across biological barriers, Adv. Mater. (2011)https://doi.org/10.1002/adma.201102313.
[13] X. Wang, L. Yang, Z. Chen, D.M. Shin, Application of nanotechnology in cancer therapy and imaging, CA. Cancer J. Clin. (2008)https://doi.org/10.3322/CA.2007.0003.
[14] J. Liu, Y. Lu, Smart nanomaterials responsive to multiple chemical stimuli with controllable cooperativity, Adv. Mater. (2006)https://doi.org/10.1002/adma.200600525.
[15] M. Motornov, Y. Roiter, I. Tokarev, S. Minko, Stimuli-responsive nanoparticles, nanogels and capsules for integrated multifunctional intelligent systems, Prog. Polym. Sci. (2010)https://doi.org/10.1016/j.progpolymsci.2009.10.004.
[16] K.K. Jain, Advances in the field of nanooncology, BMC Med. (2010)https://doi.org/10.1186/1741-7015-8-83.
[17] R. Cheng, F. Meng, C. Deng, H.A. Klok, Z. Zhong, Dual and multi-stimuli responsive polymeric nanoparticles for programmed site-specific drug delivery, Biomaterials. (2013)https://doi.org/10.1016/j.biomaterials.2013.01.084.
[18] Y. Wang, M.S. Shim, N.S. Levinson, H.W. Sung, Y. Xia, Stimuli-responsive materials for controlled release of theranostic agents, Adv. Funct. Mater. (2014)https://doi.org/10.1002/adfm.201400279.
[19] O. Onaca, R. Enea, D.W. Hughes, W. Meier, Stimuli-responsive polymersomes as nanocarriers for drug and gene delivery, Macromol. Biosci. (2009)https://doi.org/10.1002/mabi.200800248.
[20] G. Yang, X. Sun, J. Liu, L. Feng, Z. Liu, Light-responsive, singlet oxygen-triggered on-demand drug release from photosensitizer-doped mesoporous silica nanorods for cancer combination therapy, Adv. Funct. Mater. (2016)https://doi.org/10.1002/adfm.201600722.
[21] A. Sneider, D. VanDyke, S. Paliwal, P. Rai, Remotely triggered nano-theranostics For cancer applications, Nanotheranostics. (2017)https://doi.org/10.7150/ntno.17109.
[22] Q. Chen, H. Ke, Z. Dai, Z. Liu, Nanoscale theranostics for physical stimulus-responsive cancer therapies, Biomaterials. (2015)https://doi.org/10.1016/j.biomaterials.2015.09.018.

[23] C. Sun, J.S.H. Lee, M. Zhang, Magnetic nanoparticles in MR imaging and drug delivery, Adv. Drug Deliv. Rev. (2008)https://doi.org/10.1016/j.addr.2008.03.018.
[24] P. Zhang, C. Hu, W. Ran, J. Meng, Q. Yin, Y. Li, Recent progress in light-triggered nanotheranostics for cancer treatment, Theranostics. (2016)https://doi.org/10.7150/thno.15217.
[25] D. Yoo, J.H. Lee, T.H. Shin, J. Cheon, Theranostic magnetic nanoparticles, Acc. Chem. Res. (2011)https://doi.org/10.1021/ar200085c.
[26] M. Hofmann-Amtenbrink, B. von Rechenberg, H. Hofmann, Superparamagnetic Nanoparticles for Biomedical Applications, 2009https://doi.org/10.1016/j.addr.2012.10.008.
[27] G.A. Husseini, W.G. Pitt, Micelles and nanoparticles for ultrasonic drug and gene delivery, Adv. Drug Deliv. Rev. (2008)https://doi.org/10.1016/j.addr.2008.03.008.
[28] J. Kost, K. Leong, R. Langer, Ultrasound-enhanced polymer degradation and release of incorporated substances, Proc. Natl. Acad. Sci. U. S. A. (1989)https://doi.org/10.1073/pnas.86.20.7663.
[29] A.A.M. Elsherbini, M. Saber, M. Aggag, A. El-Shahawy, H.A.A. Shokier, Laser and radiofrequency-induced hyperthermia treatment via gold-coated magnetic nanocomposites, Int. J. Nanomedicine. (2011)https://doi.org/10.2147/IJN.S23952.
[30] A. Kamkaew, F. Chen, Y. Zhan, R.L. Majewski, W. Cai, Scintillating nanoparticles as energy mediators for enhanced photodynamic therapy, ACS Nano. (2016)https://doi.org/10.1021/acsnano.6b01401.
[31] L. Cheng, C. Wang, L. Feng, K. Yang, Z. Liu, Functional nanomaterials for phototherapies of cancer, Chem. Rev. (2014)https://doi.org/10.1021/cr400532z.
[32] P. Agostinis, K. Berg, K. et al Cengel, Photodynamic therapy of cancer: An update, CA, Cancer J. Clin. 61 (2011) 250–281.
[33] S.S. Kelkar, T.M. Reineke, Theranostics: Combining imaging and therapy, Bioconjug. Chem. (2011)https://doi.org/10.1021/bc200151q.
[34] M.P. Melancon, M. Zhou, C. Li, Cancer theranostics with near-infrared light-activatable multimodal nanoparticles, Acc. Chem. Res. (2011)https://doi.org/10.1021/ar200022e.
[35] H. Kim, K. Chung, S. Lee, D.H. Kim, H. Lee, Near-infrared light-responsive nanomaterials for cancer theranostics, Wiley Interdiscip. Rev. Nanomed. Nanobiotechnol. (2016)https://doi.org/10.1002/wnan.1347.
[36] M. Karimi, P. Sahandi Zangabad, S. Baghaee-Ravari, M. Ghazadeh, H. Mirshekari, M.R. Hamblin, Smart nanostructures for cargo delivery: Uncaging and activating by light, J. Am. Chem. Soc. (2017)https://doi.org/10.1021/jacs.6b08313.
[37] X. Yang, E.W. Stein, S. Ashkenazi, L.V. Wang, Nanoparticles for photoacoustic imaging, Wiley Interdiscip. Rev. Nanomedicine Nanobiotechnology. (2009)https://doi.org/10.1002/wnan.42.
[38] M. Haase, H. Schäfer, Upconverting nanoparticles, Angew. Chemie - Int. Ed. (2011) https://doi.org/10.1002/anie.201005159.
[39] S. Harmsen, M.A. Wall, R. Huang, M.F. Kircher, Cancer imaging using surface-enhanced resonance Raman scattering nanoparticles, Nat. Protoc. (2017)https://doi.org/10.1038/nprot.2017.031.
[40] J.R. Melamed, R.S. Edelstein, E.S. Day, Elucidating the fundamental mechanisms of cell death triggered by photothermal therapy, ACS Nano. (2015)https://doi.org/10.1021/acsnano.5b00021.
[41] E.S. Day, J.G. Morton, J.L. West, Nanoparticles for thermal cancer therapy, J. Biomech. Eng. (2009)https://doi.org/10.1115/1.3156800.
[42] N.A. Koonce, C.M. Quick, M.E. Hardee, A. Jamshidi-Parsian, J.A. Dent, G.F. Paciotti, D. Nedosekin, R.P.M. Dings, R.J. Griffin, Combination of gold nanoparticle-conjugated tumor necrosis factor-α and radiation therapy results in a synergistic antitumor response in murine carcinoma models, Int. J. Radiat. Oncol. Biol. Phys. (2015)https://doi.org/10.1016/j.ijrobp.2015.07.2275.
[43] M. Orecchioni, R. Cabizza, A. Bianco, L.G. Delogu, Graphene as cancer theranostic tool: Progress and future challenges, Theranostics. (2015)https://doi.org/10.7150/thno.11387.
[44] Z. Lin, Y. Liu, X. Ma, S. Hu, J. Zhang, Q. Wu, W. Ye, S. Zhu, D. Yang, D. Qu, J. Jiang, Photothermal ablation of bone metastasis of breast cancer using PEGylated multi-walled carbon nanotubes, Sci. Rep. (2015)https://doi.org/10.1038/srep11709.
[45] X. Tu, Y. Ma, Y. Cao, J. Huang, M. Zhang, Z. Zhang, PEGylated carbon nanoparticles for efficient in vitro photothermal cancer therapy, J. Mater. Chem. B. (2014)https://doi.org/10.1039/C3TB21750G.
[46] W. Yin, L. Yan, J. Yu, G. Tian, L. Zhou, X. Zheng, X. Zhang, Y. Yong, J. Li, Z. Gu, Y. Zhao, High-throughput synthesis of single-layer MoS_2 nanosheets as a near-infrared photothermal-triggered drug delivery for effective cancer therapy, ACS Nano. (2014)https://doi.org/10.1021/nn501647j.
[47] T. Liu, C. Wang, X. Gu, H. Gong, L. Cheng, X. Shi, L. Feng, B. Sun, Z. Liu, Drug Delivery with PEGylated MoS_2 nano-sheets for combined photothermal and chemotherapy of cancer, Adv. Mater. (2014)https://doi.org/10.1002/adma.201305256.
[48] G. Song, C. Liang, H. Gong, M. Li, X. Zheng, L. Cheng, K. Yang, X. Jiang, Z. Liu, Core-shell MnSe@Bi_2Se_3 fabricated via a cation exchange method as novel nanotheranostics for multimodal imaging and synergistic thermoradiotherapy, Adv. Mater. (2015)https://doi.org/10.1002/adma.201503006.
[49] S. Jana, B.B. Srivastava, S. Jana, R. Bose, N. Pradhan, Multifunctional doped semiconductor nanocrystals, J. Phys. Chem. Lett. (2012)https://doi.org/10.1027/jz3010877.
[50] NCT00356980: TNF-Bound Colloidal Gold in Treating Patients with Advanced Solid Tumors
[51] I. Iltis, J. Choi, M. Vollmers, M. Shenoi, J. Bischof, G.J. Metzger, In vivo detection of the effects of preconditioning on LNCaP tumors by a TNF-α nanoparticle construct using MRI, NMR Biomed. (2014)https://doi.org/10.1002/nbm.3157.
[52] NCT00848042: Pilot Study of AuroLase (tm) Therapy in Refractory and/or Recurrent Tumors of the Head and Neck
[53] NCT01679470: Efficacy Study of AuroLase Therapy in Subjects With Primary and/or Metastatic Lung Tumors.
[54] L.R. Hirsch, R.J. Stafford, J.A. Bankson, S.R. Sershen, B. Rivera, R.E. Price, J.D. Hazle, N.J. Halas, J.L. West, Nanoshell-mediated near-infrared thermal therapy of tumors under magnetic resonance guidance, Proc. Natl. Acad. Sci. (2003)https://doi.org/10.1073/pnas.2232479100.
[55] J.A. Schwartz, A.M. Shetty, R.E. Price, R.J. Stafford, J.C. Wang, R.K. Uthamanthil, K. Pham, R.J. McNichols, C.L. Coleman, J.D. Payne, Feasibility study of particle-assisted laser ablation of brain tumors in orthotopic canine model, Cancer Res. (2009)https://doi.org/10.1158/0008-5472.CAN-08-2535.
[56] J.M. Stern, J. Stanfield, W. Kabbani, J.T. Hsieh, J.A. Cadeddu, Selective prostate cancer thermal ablation with laser activated gold nanoshells, J. Urol. (2008)https://doi.org/10.1016/j.juro.2007.09.018.
[57] P. Diagaradjane, A. Shetty, J.C. Wang, A.M. Elliott, J. Schwartz, S. Shentu, H.C. Park, A. Deorukhkar, R.J. Stafford, S.H. Cho, J.W. Tunnell, J.D. Hazle, S. Krishnan, Modulation of in vivo tumor radiation response via gold nanoshell-mediated vascular-focused hyperthermia: Characterizing an integrated antihypoxic and localized vascular disrupting targeting strategy, Nano Lett. (2008)https://doi.org/10.1021/nl080496z.
[58] NCT02680535: MRI/US Fusion Imaging and Biopsy in Combination With Nanoparticle Directed Focal Therapy for Ablation of Prostate Tissue.
[59] NCT01270139: Plasmonic Nanophotothermal Therapy of Atherosclerosis (NANOM-FIM).
[60] Y. Hu, C. Chi, S. Wang, L. Wang, P. Liang, F. Liu, W. Shang, W. Wang, F. Zhang, S. Li, H. Shen, X. Yu, H. Liu, J. Tan, A comparative study of clinical intervention and interventional photothermal therapy for pancreatic cancer, Adv. Mater. (2017)https://doi.org/10.1002/adma.201700448.
[61] E.Y. Lukianova-Hleb, Y.S. Kim, I. Belatsarkouski, A.M. Gillenwater, D.O. Lapotko Neill, Intraoperative diagnostics and elimination of residual microtumours with plasmonic nanobubbles, Nat. Nanotechnol. 11 (2016) 525–532.
[62] E.Y. Lukianova-Hleb, X. Ren, J.A. Zasadzinski, X. Wu, D.O. Lapotko, Plasmonic nanobubbles enhance efficacy and selectivity of chemotherapy against drug-resistant cancer cells, Adv. Mater. (2012)https://doi.org/10.1002/adma.201103550.
[63] J. Tang, X. Jiang, L. Wang, H. Zhang, Z. Hu, Y. Liu, X. Wu, C. Chen, Au@Pt nanostructures: A novel photothermal conversion agent for cancer therapy, Nanoscale. (2014)https://doi.org/10.1039/c3nr06841b.
[64] J.T. Robinson, S.M. Tabakman, Y. Liang, H. Wang, H. Sanchez Casalongue, D. Vinh, H. Dai, Ultrasmall reduced graphene oxide with high near-infrared absorbance for photothermal therapy, J. Am. Chem. Soc. (2011)https://doi.org/10.1021/ja2010175.
[65] X. Ding, C.H. Liow, M. Zhang, R. Huang, C. Li, H. Shen, M. Liu, Y. Zou, N. Gao, Z. Zhang, Y. Li, Q. Wang, S. Li, J. Jiang, Surface plasmon resonance enhanced light absorption and photothermal therapy in the second near-infrared window, J. Am. Chem. Soc. (2014)https://doi.org/10.1021/ja508641z.
[66] Q. Tian, J. Hu, Y. Zhu, R. Zou, Z. Chen, S. Yang, R. Li, Q. Su, Y. Han, X. Liu, Sub-10 nm Fe_3O_4@$Cu_{2-x}S$ core-shell nanoparticles for dual-modal imaging and photothermal therapy, J. Am. Chem. Soc. (2013)https://doi.org/10.1021/ja4013497.
[67] Z. Huang, A review of progress in clinical photodynamic therapy, Technol. Cancer Res. Treat. (2005)https://doi.org/10.1177/153303460500400308.
[68] D.E.J.G.J. Dolmans, D. Fukumura, R.K. Jain, Photodynamic therapy for cancer, Nat. Rev. Cancer. (2003)https://doi.org/10.1038/nrc1071.
[69] C.A. Robertson, D.H. Evans, H. Abrahamse, Photodynamic therapy (PDT): A short review on cellular mechanisms and cancer research applications for PDT, J. Photochem. Photobiol. B Biol. (2009)https://doi.org/10.1016/j.jphotobiol.2009.04.001.
[70] J. Zhang, C. Jiang, J.P. Figueiró Longo, R.B. Azevedo, H. Zhang, L.A. Muehlmann, An updated overview on the development of new photosensitizers for anticancer photodynamic therapy, Acta Pharm. Sin. B. (2018)https://doi.org/10.1016/j.apsb.2017.09.003.
[71] R.R. Allison, G.H. Downie, R. Cuenca, X.H. Hu, C.J.H. Childs, C.H. Sibata, Photosensitizers in clinical PDT, Photodiagnosis Photodyn. Ther. (2004).
[72] H. Abrahamse, M.R. Hamblin, New photosensitizers for photodynamic therapy, Biochem. J. (2016)https://doi.org/10.1042/BJ20150942.
[73] G. Tian, X. Zhang, Z. Gu, Y. Zhao, Recent advances in upconversion nanoparticles-based multifunctional nanocomposites for combined cancer therapy, Adv. Mater. (2015)https://doi.org/10.1002/adma.201503280.
[74] G. Chen, H. Qiu, P.N. Prasad, X. Chen, Upconversion nanoparticles: Design, nanochemistry, and applications in Theranostics, Chem. Rev. (2014)https://doi.org/10.1021/cr400425h.
[75] F. Ai, Q. Ju, X. Zhang, X. Chen, F. Wang, G. Zhu, A core-shell-shell nanoplatform upconverting near-infrared light at 808 nm for luminescence imaging and photodynamic therapy of cancer, Sci. Rep. (2015)https://doi.org/10.1038/srep10785.
[76] Z. Hou, Y. Zhang, K. Deng, Y. Chen, X. Li, X. Deng, Z. Cheng, H. Lian, C. Li, J. Lin, UV-emitting upconversion-based TiO2photosensitizing nanoplatform: Near-infrared light mediated in vivo photodynamic therapy via mitochondria-involved apoptosis pathway, ACS Nano. (2015)https://doi.org/10.1021/nn506107c.
[77] L. Zhang, L. Zeng, Y. Pan, S. Luo, W. Ren, A. Gong, X. Ma, H. Liang, G. Lu, A. Wu, Inorganic photosensitizer coupled Gd-based upconversion luminescent nanocomposites for in vivo magnetic resonance imaging and near-infrared-responsive photodynamic therapy in cancers, Biomaterials. (2015)https://doi.org/10.1016/j.biomaterials.2014.12.040.
[78] A. Punjabi, X. Wu, A. Tokatli-Apollon, M. El-Rifai, H. Lee, Y. Zhang, C. Wang, Z. Liu, E.M. Chan, C. Duan, G. Han, Amplifying the red-emission of upconverting nanoparticles for biocompatible clinically used prodrug-induced photodynamic therapy, ACS Nano. (2014)https://doi.org/10.1021/nn505051d.
[79] L. Zeng, Y. Pan, Y. Tian, X. Wang, W. Ren, S. Wang, G. Lu, A. Wu, Doxorubicin-loaded $NaYF_4$:Yb/Tm–TiO_2 inorganic photosensitizers for NIR-triggered photodynamic

therapy and enhanced chemotherapy in drug-resistant breast cancers, Biomaterials. (2015)https://doi.org/10.1016/j.biomaterials.2015.04.006.
[80] S. Cui, D. Yin, Y. Chen, Y. Di, H. Chen, Y. Ma, S. Achilefu, Y. Gu, In vivo targeted deep-tissue photodynamic therapy based on near-infrared light triggered upconversion nanoconstruct, ACS Nano. (2013)https://doi.org/10.1021/nn304872n.
[81] S. Wang, A. Riedinger, H. Li, C. Fu, H. Liu, L. Li, T. Liu, L. Tan, M.J. Barthel, G. Pugliese, F. De Donato, M. Scotto, X. D'Abbusco, L. Meng, H. Manna, T. Pellegrino Meng, Plasmonic copper sulfide nanocrystals exhibiting near-infrared photothermal and photodynamic therapeutic effects, ACS Nano. (2015)https://doi.org/10.1021/nn506687t.
[82] R. Vankayala, C.C. Lin, P. Kalluru, C.S. Chiang, K.C. Hwang, Gold nanoshells-mediated bimodal photodynamic and photothermal cancer treatment using ultra-low doses of near infra-red light, Biomaterials. (2014)https://doi.org/10.1016/j.biomaterials.2014.03.065.
[83] W. Guo, Z. Qiu, C. Guo, D. Ding, T. Li, F. Wang, J. Sun, N. Zheng, S. Liu, Multifunctional theranostic agent of $Cu_2(OH)PO_4$ quantum dots for photoacoustic image-guided photothermal/photodynamic combination cancer therapy, ACS Appl. Mater. Interfaces. (2017)https://doi.org/10.1021/acsami.6b15703.
[84] Y. Chen, H. Li, Y. Deng, H. Sun, X. Ke, T. Ci, Near-infrared light triggered drug delivery system for higher efficacy of combined chemo-photothermal treatment, Acta Biomater. (2017)https://doi.org/10.1016/j.actbio.2016.12.004.
[85] C. Yue, C. Zhang, G. Alfranca, Y. Yang, X. Jiang, Y. Yang, F. Pan, J.M. de la Fuente, D. Cui, Near-infrared light triggered ROS-activated theranostic platform based on Ce6-CPT-UCNPs for simultaneous fluorescence imaging and chemo-photodynamic combined therapy, Theranostics. (2016)https://doi.org/10.7150/thno.14101.
[86] Y. Ma, X. Liang, S. Tong, G. Bao, Q. Ren, Z. Dai, Gold nanoshell nanomicelles for potential magnetic resonance imaging, light-triggered drug release, and photothermal therapy, Adv. Funct. Mater. (2013)https://doi.org/10.1002/adfm.201201663.
[87] J. Liu, C. Wang, X. Wang, X. Wang, L. Cheng, Y. Li, Z. Liu, Mesoporous silica coated single-walled carbon nanotubes as a multifunctional light-responsive platform for cancer combination therapy, Adv. Funct. Mater. (2015)https://doi.org/10.1002/adfm.201403079.
[88] A.M. Goodman, O. Neumann, K. Nørregaard, L. Henderson, M.-R. Choi, S.E. Clare, N.J. Halas, Near-infrared remotely triggered drug-release strategies for cancer treatment, Proc. Natl. Acad. Sci. (2017)https://doi.org/10.1073/pnas.1713137114.
[89] A.M. Pekkanen, M.R. DeWitt, M.N. Rylander, Nanoparticle enhanced optical imaging and phototherapy of cancer, J. Biomed. Nanotechnol. (2014)https://doi.org/10.1166/jbn.2014.1988.
[90] S. Luo, E. Zhang, Y. Su, T. Cheng, C. Shi, A review of NIR dyes in cancer targeting and imaging, Biomaterials. (2011)https://doi.org/10.1016/j.biomaterials.2011.06.024.
[91] C.T. Xu, Q.Q. Zhan, H.C. Liu, G. Somesfalean, J. Qian, S.L. He, S. Andersson-Engels, Upconverting nanoparticles for pre-clinical diffuse optical imaging, microscopy and sensing: Current trends and future challenges, Laser Photon. Rev. (2013)https://doi.org/10.1002/lpor.201200052.
[92] G. Tian, X. Zheng, X. Zhang, W. Yin, J. Yu, D. Wang, Z. Zhang, X. Yang, Z. Gu, Y. Zhao, TPGS-stabilized $NaYbF_4$:ER Upconversion nanoparticles for dual-modal fluorescent/CT imaging and anticancer drug delivery to overcome multi-drug resistance, Biomaterials. (2015)https://doi.org/10.1016/j.biomaterials.2014.11.022.
[93] M.S. Muthu, R.V. Kutty, Z. Luo, J. Xie, S.S. Feng, Theranostic vitamin E TPGS micelles of transferrin conjugation for targeted co-delivery of docetaxel and ultra bright gold nanoclusters, Biomaterials. (2015)https://doi.org/10.1016/j.biomaterials.2014.11.008.
[94] S.N. Baker, G.A. Baker, Luminescent carbon nanodots: Emergent nanolights, Angew. Chemie - Int. Ed. (2010)https://doi.org/10.1002/anie.200906623.
[95] X. Wang, L. Cao, F. Lu, M.J. Meziani, H. Li, G. Qi, B. Zhou, B.A. Harruff, F. Kermarrec, Y.-P. Sun, Photoinduced electron transfers with carbon dots, Chem. Commun. (Camb). (2009)https://doi.org/10.1039/b906252a.
[96] C. Li, Y. Zhang, M. Wang, Y. Zhang, G. Chen, D. Wu, Q. Wang, In vivo real-time visualization of tissue blood flow and angiogenesis using Ag_2S quantum dots in the NIR-II window, Biomaterials. (2014)https://doi.org/10.1016/j.biomaterials.2013.10.010.
[97] X. Sun, X. Huang, X. Yan, Y. Wang, J. Guo, O. Jacobson, D. Liu, L.P. Szajek, W. Zhu, G. Niu, D.O. Kiesewetter, S. Sun, X. Chen, Chelator-free 64Cu-integrated gold nanomaterials for positron emission tomography imaging guided photothermal cancer therapy, ACS Nano. (2014)https://doi.org/10.1021/nn502950t.
[98] W. Zhang, Y. Wang, X. Sun, W. Wang, L. Chen, Mesoporous titania based yolk-shell nanoparticles as multifunctional theranostic platforms for SERS imaging and chemo-photothermal treatment, Nanoscale. (2014)https://doi.org/10.1039/c4nr04864d.
[99] P. Beard, Biomedical photoacoustic imaging, Interface Focus. (2011)https://doi.org/10.1098/rsfs.2011.0028.
[100] S. Mallidi, G.P. Luke, S. Emelianov, Photoacoustic imaging in cancer detection, diagnosis, and treatment guidance, Trends Biotechnol. (2011)https://doi.org/10.1016/j.tibtech.2011.01.006.
[101] W. Li, X. Chen, Gold nanoparticles for photoacoustic imaging, Nanomedicine (Lond) (2015)https://doi.org/10.2217/nnm.14.169.
[102] S. Ye, G. Marston, J.R. McLaughlan, D.O. Sigle, N. Ingram, S. Freear, J.J. Baumberg, R.J. Bushby, A.F. Markham, K. Critchley, P.L. Coletta, S.D. Evans, Engineering gold nanotubes with controlled length and near-infrared absorption for theranostic applications, Adv. Funct. Mater. (2015)https://doi.org/10.1002/adfm.201404358.
[103] H. Ding, J.S. Wei, N. Zhong, Q.Y. Gao, H.M. Xiong, Highly efficient red-emitting carbon dots with gram-scale yield for bioimaging, Langmuir. (2017)https://doi.org/10.1021/acs.langmuir.7b02385.
[104] J. Song, X. Yang, O. Jacobson, P. Huang, X. Sun, L. Lin, X. Yan, G. Niu, Q. Ma, X. Chen, Ultrasmall gold nanorod vesicles with enhanced tumor accumulation and fast excretion from the body for cancer therapy, Adv. Mater. (2015)https://doi.org/10.1002/adma.201502486.
[105] M.F. Kircher, A. De La Zerda, J.V. Jokerst, C.L. Zavaleta, P.J. Kempen, E. Mittra, K. Pitter, R. Huang, C. Campos, F. Habte, R. Sinclair, C.W. Brennan, I.K. Mellinghoff, E.C. Holland, S.S. Gambhir, A brain tumor molecular imaging strategy using a new triple-modality MRI-photoacoustic-Raman nanoparticle, Nat. Med. (2012)https://doi.org/10.1038/nm.2721.
[106] L. Zhang, S. Gao, F. Zhang, K. Yang, Q. Ma, L. Zhu, Activatable hyaluronic acid nanoparticle as a theranostic agent for optical/photoacoustic image-guided photothermal therapy, ACS Nano. (2014)https://doi.org/10.1021/nn506130t.
[107] L.H. Reddy, J.L. Arias, J. Nicolas, P. Couvreur, Magnetic nanoparticles: Design and characterization, toxicity and biocompatibility, pharmaceutical and biomedical applications, Chem. Rev. (2012)https://doi.org/10.1021/cr300068p.
[108] S. Laurent, D. Forge, M. Port, A. Roch, C. Robic, L. Vander Elst, R.N. Muller, Magnetic iron oxide nanoparticles: Synthesis, stabilization, vectorization, physicochemical characterizations and biological applications, Chem. Rev. (2008)https://doi.org/10.1021/cr068445e.
[109] M. Bañobre-López, A. Teijeiro, J. Rivas, Magnetic nanoparticle-based hyperthermia for cancer treatment, Reports Pract. Oncol. Radiother. (2013)https://doi.org/10.1016/j.rpor.2013.09.011.
[110] Z. Hedayatnasab, F. Abnisa, W.M.A.W. Daud, Review on magnetic nanoparticles for magnetic nanofluid hyperthermia application, Mater. Des. (2017)https://doi.org/10.1016/j.matdes.2017.03.036.
[111] M. Angelakeris, Magnetic nanoparticles: A multifunctional vehicle for modern theranostics, Biochim. Biophys. Acta - Gen. Subj. (2017)https://doi.org/10.1016/j.bbagen.2017.02.022.
[112] NCT02033447: Magnetic Nanoparticle Thermoablation-Retention and Maintenance in the Prostate: A Phase 0 Study in Men (MAGNABLATE I).
[113] DRKS00005476: MF 1001: Open-label, randomized, controlled study to determine the efficacy and safety of NanoTherm® monotherapy and NanoTherm® in combination with radiotherapy versus radiotherapy alone in recurrent / progressive glioblastoma.
[114] M. Johannsen, U. Gneveckow, K. Taymoorian, B. Thiesen, N. Waldöfner, R. Scholz, K. Jung, A. Jordan, P. Wust, S.A. Loening, Morbidity and quality of life during thermotherapy using magnetic nanoparticles in locally recurrent prostate cancer: Results of a prospective phase I trial, Int. J. Hyperth. (2007)https://doi.org/10.1080/02656730601175479.
[115] K. Maier-Hauff, R. Rothe, R. Scholz, U. Gneveckow, P. Wust, B. Thiesen, A. Feussner, A. Deimling, N. Waldoefner, R. Felix, A. Jordan, Intracranial thermotherapy using magnetic nanoparticles combined with external beam radiotherapy: Results of a feasibility study on patients with glioblastoma multiforme, J. Neurooncol. (2007)https://doi.org/10.1007/s11060-006-9195-0.
[116] A. Matsumine, K. Takegami, K. Asanuma, T. Matsubara, T. Nakamura, A. Uchida, A. Sudo, A novel hyperthermia treatment for bone metastases using magnetic materials, Int. J. Clin. Oncol. (2011)https://doi.org/10.1007/s10147-011-0217-3.
[117] L. Yu, J. Liu, K. Wu, T. Klein, Y. Jiang, J.P. Wang, Evaluation of hyperthermia of magnetic nanoparticles by dehydrating DNA, Sci. Rep. (2014)https://doi.org/10.1038/srep07216.
[118] V. Kumar, Y. Gu, S. Basu, A. Berglund, S.A. Eschrich, M.B. Schabath, K. Forster, H.J.W.L. Aerts, A. Dekker, D. Fenstermacher, D.B. Goldgof, L.O. Hall, P. Lambin, Y. Balagurunathan, R.A. Gatenby, R.J. Gillies, Radiomics: The process and the challenges, Magn. Reson. Imaging. (2012)https://doi.org/10.1016/j.mri.2012.06.010.
[119] J.Y. Lee, J.H. Kim, K.H. Bae, M.H. Oh, Y. Kim, J.S. Kim, T.G. Park, K. Park, J.H. Lee, Y.S. Nam, Low-density lipoprotein-mimicking nanoparticles for tumor-targeted theranostic applications, Small. (2015)https://doi.org/10.1002/smll.201303277.
[120] P.M. Matthews, P. Jezzard, Functional magnetic resonance imaging, J. Neurol. Neurosurg. Psychiatry. 75 (2004) 6–12.
[121] C.L. Degen, M. Poggio, H.J. Mamin, C.T. Rettner, D. Rugar, Nanoscale magnetic resonance imaging, Proc. Natl. Acad. Sci. U. S. A. (2009)https://doi.org/10.1073/pnas.0812068106.
[122] Y.X.J. Wang, S.M. Hussain, G.P. Krestin, Superparamagnetic iron oxide contrast agents: Physicochemical characteristics and applications in MR imaging, Eur. Radiol. (2001)https://doi.org/10.1007/s003300100908.
[123] S. Zanganeh, G. Hutter, R. Spitler, O. Lenkov, M. Mahmoudi, A. Shaw, J.S. Pajarinen, H. Nejadnik, S. Goodman, M. Moseley, L.M. Coussens, H.E. Daldrup-Link, Iron oxide nanoparticles inhibit tumour growth by inducing pro-inflammatory macrophage polarization in tumour tissues, Nat. Nanotechnol. (2016)https://doi.org/10.1038/nnano.2016.168.
[124] A.L. Cortajarena, D. Ortega, S.M. Ocampo, A. Gonzalez-García, P. Couleaud, R. Miranda, C. Belda-Iniesta, A. Ayuso-Sacido, Engineering iron oxide nanoparticles for clinical settings, Nanobiomedicine. (2014)https://doi.org/10.5772/58841.
[125] B.E. Hamilton, G.M. Nesbit, E. Dosa, S. Gahramanov, B. Rooney, E.G. Nesbit, J. Raines, E.A. Neuwelt, Comparative analysis of ferumoxytol and gadoteridol enhancement using T1- and T2-weighted MRI in neuroimaging, Am. J. Roentgenol. (2011)https://doi.org/10.2214/AJR.10.5992.
[126] M.G. Harisinghani, J. Barentsz, P.F. Hahn, W.M. Deserno, S. Tabatabaei, C.H. van de Kaa, J. de la Rosette, R. Weissleder, Noninvasive detection of clinically occult lymph-node metastases in prostate cancer, N. Engl. J. Med. (2003)https://doi.org/10.1056/NEJMoa022749.
[127] Y. Chen, Q. Zhu, Y. Tian, W. Tang, F. Pan, R. Xiong, Y. Yuan, A. Hu, Supramolecular aggregates from polyacrylates and Gd(III)-containing cationic surfactants as high-relaxivity MRI contrast agents, Polym. Chem. (2015)https://doi.org/10.1039/c4py01562b.

[128] K.M.L. Taylor, J.S. Kim, W.J. Rieter, H. An, W. Lin, W. Lin, Mesoporous silica nanospheres as highly efficient MRI contrast agents, J. Am. Chem. Soc. (2008)https://doi.org/10.1021/ja710193c.
[129] D. Pan, S.D. Caruthers, A. Senpan, A.H. Schmieder, S.A. Wickline, G.M. Lanza, Revisiting an old friend: Manganese-based MRI contrast agents, Wiley Interdiscip. Rev. Nanomedicine Nanobiotechnology. (2011)https://doi.org/10.1002/wnan.116.
[130] Y. Cheng, S. Zhang, N. Kang, J. Huang, X. Lv, K. Wen, S. Ye, Z. Chen, X. Zhou, L. Ren, Polydopamine-coated manganese carbonate nanoparticles for amplified magnetic resonance imaging-guided photothermal therapy, ACS Appl. Mater. Interfaces. (2017)https://doi.org/10.1021/acsami.7b03087.
[131] Y. Luo, J. Yang, Y. Yan, J. Li, M. Shen, G. Zhang, S. Mignani, X. Shi, RGD-functionalized ultrasmall iron oxide nanoparticles for targeted T1-weighted MR imaging of gliomas, Nanoscale. (2015)https://doi.org/10.1039/c5nr04003e.
[132] D. Bates, S. Abraham, M. Campbell, I. Zehbe, L. Curiel, Development and characterization of an antibody-labeled super-paramagnetic iron oxide contrast agent targeting prostate cancer cells for magnetic resonance imaging, PLoS One. (2014) https://doi.org/10.1371/journal.pone.0097220.
[133] V.V. Mody, A. Cox, S. Shah, A. Singh, W. Bevins, H. Parihar, Magnetic nanoparticle drug delivery systems for targeting tumor, Appl. Nanosci. (2013)https://doi.org/10.1007/s13204-013-0216-y.
[134] T.Y. Liu, K.H. Liu, D.M. Liu, S.Y. Chen, I.W. Chen, Temperature-sensitive nanocapsules for controlled drug release caused by magnetically triggered structural disruption, Adv. Funct. Mater. (2009)https://doi.org/10.1002/adfm.200801304.
[135] S. Kayal, R.V. Ramanujan, Doxorubicin loaded PVA coated iron oxide nanoparticles for targeted drug delivery, Mater. Sci. Eng. C. (2010)https://doi.org/10.1016/j.msec.2010.01.006.
[136] X. Hua, Q. Yang, Z. Dong, J. Zhang, W. Zhang, Q. Wang, S. Tan, H.D.C. Smyth, Magnetically triggered drug release from nanoparticles and its applications in anti-tumor treatment, Drug Deliv. (2017)https://doi.org/10.1080/10717544.2016.1256001.
[137] C. Sanson, O. Diou, J. Thévenot, E. Ibarboure, A. Soum, A. Brûlet, S. Miraux, E. Thiaudière, S. Tan, A. Brisson, V. Dupuis, O. Sandre, S. Lecommandoux, Doxorubicin loaded magnetic polymersomes: Theranostic nanocarriers for MR imaging and magneto-chemotherapy, ACS Nano. (2011)https://doi.org/10.1021/nn102762f.
[138] J. Powers, F. Kremkau, Medical ultrasound systems, Interface Focus. (2011)https://doi.org/10.1098/rsfs.2011.0027.
[139] J.A. Jensen, Medical ultrasound imaging, Prog. Biophys. Mol. Biol. (2007)https://doi.org/10.1016/j.pbiomolbio.2006.07.025.
[140] G. Canavese, A. Ancona, L. Racca, M. Canta, B. Dumontel, F. Barbaresco, T. Limongi, V. Cauda, Nanoparticle-assisted ultrasound: A special focus on sonodynamic therapy against cancer, Chem. Eng. J. (2018)https://doi.org/10.1016/j.cej.2018.01.060.
[141] Y.-Z. Zhao, L.-N. Du, C.-T. Lu, Y.-G. Jin, S.-P. Ge, Potential and problems in ultrasound-responsive drug delivery systems, Int. J. Nanomedicine. (2013) https://doi.org/10.2147/IJN.S43589.
[142] L. Fu, H.-T. Ke, L. Fu, H.-T. Ke, Nanomaterials incorporated ultrasound contrast agents for cancer theranostics, Cancer Biol. Med. (2016)https://doi.org/10.20892/j.issn.2095-3941.2016.0065.
[143] T.F. Shklyar, O.A. Toropova, A.P. Safronov, D.V. Leiman, Y.A. Kotov, F.A. Blyakhman, Acoustic properties of metal oxides aqueous suspensions, Nanotechnologies Russ. (2010)https://doi.org/10.1134/S1995078010030110.
[144] F. Chiriacò, G. Soloperto, A. Greco, F.-C. Conversano, A. Ragusa, L. Menichetti, S. Casciaro, F.-C. Conversano, Magnetically-coated silica nanospheres for dual-mode imaging at low ultrasound frequency, World J Radiol. (2013)https://doi.org/10.4329/wjr.v5.i11.411.
[145] J.V. Jokerst, C. Khademi, S.S. Gambhir, Intracellular aggregation of multimodal silica nanoparticles for ultrasound-guided stem cell implantation, Sci. Transl. Med. (2013)https://doi.org/10.1126/scitranslmed.3005228.
[146] F. Foroutan, J.V. Jokerst, S.S. Gambhir, O. Vermesh, H.W. Kim, J.C. Knowles, Sol-gel synthesis and electrospraying of biodegradable $(P_2O_5)_{55}$-$(CaO)_{30}$-$(Na_2O)_{15}$ glass nanospheres as a transient contrast agent for ultrasound stem cell imaging, ACS Nano. 9 (2015) 1868–1877.
[147] K. Zhang, H. Chen, Y. Zheng, Y. Chen, M. Ma, X. Wang, L. Wang, D. Zeng, J. Shi, A facile in situ hydrophobic layer protected selective etching strategy for the synchronous synthesis/modification of hollow or rattle-type silica nanoconstructs, J. Mater. Chem. (2012)https://doi.org/10.1039/c2jm31504a.
[148] F. Yang, S. Hu, Y. Zhang, X. Cai, Y. Huang, F. Wang, S. Wen, G. Teng, N. Gu, A hydrogen peroxide-responsive O_2 nanogenerator for ultrasound and magnetic-resonance dual modality imaging, Adv. Mater. (2012)https://doi.org/10.1002/adma.201202367.
[149] P. Prasad, C.R. Gordijo, A.Z. Abbasi, A. Maeda, A. Ip, M. Rauth, R.S. Dacosta, X.Y. Wu, Multifunctional albumin MnO_2 nanoparticles modulate solid tumor microenvironment by attenuating enhance radiation response, ACS Nano. (2013).
[150] K.H. Min, H.S. Min, H.J. Lee, D.J. Park, J.Y. Yhee, K. Kim, I.C. Kwon, S.Y. Jeong, O.F. Silvestre, X. Chen, Y.S. Hwang, E.C. Kim, S.C. Lee, PH-controlled gas-generating mineralized nanoparticles: A theranostic agent for ultrasound imaging and therapy of cancers, ACS Nano. (2015)https://doi.org/10.1021/nn506210a.
[151] Y.-H. Wang, A.-H. Liao, J.-H. Chen, C.-R. Chris Wang, P.-C. Li, Photoacoustic/ultrasound dual-modality contrast agent and its application to thermotherapy, J. Biomed. Opt. (2012)https://doi.org/10.1117/1.JBO.17.4.045001.
[152] H. Ke, J. Wang, Z. Dai, Y. Jin, E. Qu, Z. Xing, C. Guo, X. Yue, J. Liu, Gold-nanoshelled microcapsules: A theranostic agent for ultrasound contrast imaging and photothermal therapy, Angew. Chemie - Int. Ed. (2011)https://doi.org/10.1002/anie.201008286.
[153] G.D. Moon, S.W. Choi, X. Cai, W. Li, E.C. Cho, U. Jeong, L.V. Wang, Y. Xia, A new theranostic system based on gold nanocages and phase-change materials with unique features for photoacoustic imaging and controlled release, J. Am. Chem. Soc. (2011)https://doi.org/10.1021/ja200894u.
[154] Y. Ni, S. Mulier, Y. Miao, L. Michel, G. Marchal, A review of the general aspects of radiofrequency ablation, Abdom. Imaging. (2005)https://doi.org/10.1007/s00261-004-0253-9.
[155] E.S. Glazer, S.A. Curley, Non-invasive radiofrequency ablation of malignancies mediated by quantum dots, gold nanoparticles and carbon nanotubes, Ther. Deliv. (2011)https://doi.org/10.4155/tde.11.102.
[156] M. Raoof, S.J. Corr, W.D. Kaluarachchi, K.L. Massey, K. Briggs, C. Zhu, M.A. Cheney, L.J. Wilson, S.A. Curley, Stability of antibody-conjugated gold nanoparticles in the endolysosomal nanoenvironment: Implications for noninvasive radiofrequency-based cancer therapy, Nanomedicine Nanotechnology, Biol. Med. (2012)https://doi.org/10.1016/j.nano.2012.02.001.
[157] C.J. Gannon, P. Cherukuri, B.I. Yakobson, L. Cognet, J.S. Kanzius, C. Kittrell, R.B. Weisman, M. Pasquali, H.K. Schmidt, R.E. Smalley, S.A. Curley, Carbon nanotube-enhanced thermal destruction of cancer cells in a noninvasive radiofrequency field, Cancer. 110 (2007) 2654–2665.
[158] A.A.M. Elsherbini, M. Saber, M. Aggag, A. El-Shahawy, H.A.A. Shokier, Laser and radiofrequency-induced hyperthermia treatment via gold-coated magnetic nanocomposites, Int. J. Nanomedicine. (2011)https://doi.org/10.2147/IJN.S23952.
[159] L. Wang, P. Zhang, J. Shi, Y. Hao, D. Meng, Y. Zao, Y. Yanyan, D. Li, J. Chang, Z. Zhang, Radiofrequency-triggered tumor targeting delivery system for theranostic applications, ACS Appl. Mater. Interfaces (2015)https://doi.org/10.1021/am507898z.
[160] D. Wang, B. Lin, H. Ai, Theranostic nanoparticles for cancer and cardiovascular applications, Pharm. Res. (2014)https://doi.org/10.1007/s11095-013-1277-z.
[161] NCT01266096: PET Imaging of Patients With Melanoma and Malignant Brain Tumors Using an 124I-labeled cRGDY Silica Nanomolecular Particle Tracer: A Microdosing Study.
[162] NCT02850783: SLN in Colon Cancer Using a Multimodal Tracer.
[163] F. Chen, H. Hong, S. Goel, S.A. Graves, H. Orbay, E.B. Ehlerding, S. Shi, C.P. Theuer, R.J. Nickles, W. Cai, In vivo tumor vasculature targeting of CuS@MSN based theranostic nanomedicine, ACS Nano. (2015)https://doi.org/10.1021/nn507241v.
[164] V. Lopez-Rodriguez, R.E. Gaspar-Carcamo, M. Pedraza-Lopez, E.L. Rojas-Calderon, C. Arteaga de Murphy, G. Ferro-Flores, M.A. Avila-Rodriguez, Preparation and preclinical evaluation of ^{66}Ga-DOTA-E(c(RGDfK))$_2$ as a potential theranostic radiopharmaceutical, Nucl. Med. Biol. (2015)https://doi.org/10.1016/j.nucmedbio.2014.09.010.
[165] J. Liu, J. Han, Z. Kang, R. Golamaully, N. Xu, H. Li, X. Han, In vivo near-infrared photothermal therapy and computed tomography imaging of cancer cells using novel tungsten-based theranostic probe, Nanoscale. (2014)https://doi.org/10.1039/c3nr06292a.
[166] E. Gargioni, F. Schulz, A. Raabe, S. Burdak-Rothkamm, T. Rieckmann, K. Rothkamm, Targeted nanoparticles for tumour radiotherapy enhancement—the long dawn of a golden era? Ann. Transl. Med. (2016)https://doi.org/10.21037/atm.2016.12.46.
[167] P. Retif, S. Pinel, M. Toussaint, C. Frochot, R. Chouikrat, T. Bastogne, M. Barberi-Heyob, Nanoparticles for radiation therapy enhancement: The key parameters, Theranostics. (2015)https://doi.org/10.7150/thno.11642.
[168] NCT01433068: NBTXR3 Crystalline Nanoparticles and Radiation Therapy in Treating Patients With Soft Tissue Sarcoma of the Extremity.
[169] NCT02379845: NBTXR3 Crystalline Nanoparticles and Radiation Therapy in Treating and Randomized Patients in Two Arms With Soft Tissue Sarcoma of the Extremity and Trunk Wall.
[170] NCT02901483: A Study of PEP503 With Radiotherapy in Combination With Concurrent Chemotherapy for Patients With Head and Neck Cancer.
[171] NCT01946867: NBTXR3 Crystalline Nanoparticles and Radiation Therapy in Treating Patients With Locally Advanced Squamous Cell Carcinoma of the Oral Cavity or Oropharynx
[172] NCT02721056: NBTXR3 Crystalline Nanoparticles and Stereotactic Body Radiation Therapy in the Treatment of Liver Cancers.
[173] NCT03308604: AGuIX Gadolinium-based Nanoparticles in Combination With Chemoradiation and Brachytherapy (NANOCOL)
[174] D.Y. Joh, G.D. Kao, S. Murty, M. Stangl, L. Sun, A. Al Zaki, X. Xu, S.M. Hahn, A. Tsourkas, J.F. Dorsey, Theranostic gold nanoparticles modified for durable systemic circulation effectively and safely enhance the radiation therapy of human sarcoma cells and tumors, Transl. Oncol. (2013)https://doi.org/10.1593/tlo.13433.
[175] T. Ojha, L. Rizzo, G. Storm, F. Kiessling, T. Lammers, Image-guided drug delivery: preclinical applications and clinical translation, Expert Opin. Drug Deliv. (2015) https://doi.org/10.1517/17425247.2015.1059420.
[176] M. Ma, Y. Huang, H. Chen, X. Jia, S. Wang, Z. Wang, J. Shi, Bi_2S_3-embedded mesoporous silica nanoparticles for efficient drug delivery and interstitial radiotherapy sensitization, Biomaterials. (2015)https://doi.org/10.1016/j.biomaterials.2014.10.001.
[177] X.-D. Zhang, D. Wu, X. Shen, J. Chen, Y.-M. Sun, P.-X. Liu, X.-J. Liang, Size-dependent radiosensitization of PEG-coated gold nanoparticles for cancer radiation therapy, Biomaterials. (2012)https://doi.org/10.1016/j.biomaterials.2012.05.047.
[178] Q. Xiao, X. Zheng, W. Bu, W. Ge, S. Zhang, F. Chen, H. Xing, Q. Ren, W. Fan, K. Zhao, Y. Hua, J. Shi, A core/satellite multifunctional nanotheranostic for in vivo imaging and tumor eradication by radiation/photothermal synergistic therapy, J. Am. Chem. Soc. (2013)https://doi.org/10.1021/ja404985w.
[179] Y. Liu, W. Chen, S. Wang, A.G. Joly, Investigation of water-soluble x-ray luminescence nanoparticles for photodynamic activation, Appl. Phys. Lett. (2008)https://doi.org/10.1063/1.2835701.
[180] C. Zhang, K. Zhao, W. Bu, D. Ni, Y. Liu, J. Feng, J. Shi, Marriage of scintillator and semiconductor for synchronous radiotherapy and deep photodynamic therapy with diminished oxygen dependence, Angew. Chemie - Int. Ed. (2015)https://doi.org/10.1002/anie.201408472.

[181] S. Clement, W. Deng, E. Camilleri, B.C. Wilson, E.M. Goldys, X-ray induced singlet oxygen generation by nanoparticle-photosensitizer conjugates for photodynamic therapy: Determination of singlet oxygen quantum yield, Sci. Rep. (2016)https://doi.org/10.1038/srep19954.
[182] S. Kaščáková, A. Giuliani, S. Lacerda, A. Pallier, P. Mercère, É. Tóth, M. Réfrégiers, X-ray-induced radiophotodynamic therapy (RPDT) using lanthanide micelles: Beyond depth limitations, Nano Res. (2015)https://doi.org/10.1007/s12274-015-0747-5.
[183] W. Chen, J. Zhang, Using nanoparticles to enable simultaneous radiation and photodynamic therapies for cancer rreatment, J. Nanosci. Nanotechnol. (2006)https://doi.org/10.1166/jnn.2006.327.
[184] J. Ge, Q. Jia, W. Liu, L. Guo, Q. Liu, M. Lan, H. Zhang, X. Meng, P. Wang, Red-emissive carbon dots for fluorescent, photoacoustic, and thermal theranostics in living mice, Adv. Mater. (2015)https://doi.org/10.1002/adma.201500323.
[185] J. Ge, M. Lan, B. Zhou, W. Liu, L. Guo, H. Wang, Q. Jia, G. Niu, X. Huang, H. Zhou, X. Meng, P. Wang, C.S. Lee, W. Zhang, X. Han, A graphene quantum dot photodynamic therapy agent with high singlet oxygen generation, Nat. Commun. (2014)https://doi.org/10.1038/ncomms5596.
[186] K. Yang, S. Zhang, G. Zhang, X. Sun, S.T. Lee, Z. Liu, Graphene in mice: Ultrahigh in vivo tumor uptake and efficient photothermal therapy, Nano Lett. (2010) https://doi.org/10.1021/nl100996u.
[187] H.K. Moon, S.H. Lee, H.C. Choi, In vivo near-infrared mediated tumor destruction by photothermal effect of carbon nanotubes, ACS Nano. (2009)https://doi.org/10.1021/nn900904h.
[188] C. Liang, S. Diao, C. Wang, H. Gong, T. Liu, G. Hong, X. Shi, H. Dai, Z. Liu, Tumor metastasis inhibition by imaging-guided photothermal therapy with single-walled carbon nanotubes, Adv. Mater. (2014)https://doi.org/10.1002/adma.201401825.
[189] A.L. Antaris, J.T. Robinson, O.K. Yaghi, G. Hong, S. Diao, R. Luong, H. Dai, Ultra-low doses of chirality sorted (6,5) carbon nanotubes for simultaneous tumor imaging and photothermal therapy, ACS Nano. (2013)https://doi.org/10.1021/nn4006472.
[190] W. Miao, G. Shim, G. Kim, S. Lee, H.J. Lee, Y.B. Kim, Y. Byun, Y.K. Oh, Image-guided synergistic photothermal therapy using photoresponsive imaging agent-loaded graphene-based nanosheets, J. Control. Release (2015)https://doi.org/10.1016/j.jconrel.2015.05.280.
[191] M. Zhang, Y. Cao, Y. Chong, Y. Ma, H. Zhang, Z. Deng, C. Hu, Z. Zhang, Graphene oxide based theranostic platform for T1-weighted magnetic resonance imaging and drug delivery, ACS Appl. Mater. Interfaces. (2013)https://doi.org/10.1021/am404292e.
[192] A. Sahu, W. Il Choi, J.H. Lee, G. Tae, Graphene oxide mediated delivery of methylene blue for combined photodynamic and photothermal therapy, Biomaterials. (2013) https://doi.org/10.1016/j.biomaterials.2013.04.066.
[193] Y. Liu, J.R. Ashton, E.J. Moding, H. Yuan, J.K. Register, A.M. Fales, J. Choi, M.J. Whitley, X. Zhao, Y. Qi, Y. Ma, G. Vaidyanathan, M.R. Zalutsky, D.G. Kirsch, C.T. Badea, T. Vo-Dinh, A plasmonic gold nanostar theranostic probe for in vivo tumor imaging and photothermal therapy, Theranostics. (2015)https://doi.org/10.7150/thno.11974.
[194] P. Huang, J. Lin, W. Li, P. Rong, Z. Wang, S. Wang, X. Wang, X. Sun, M. Aronova, G. Niu, R.D. Leapman, Z. Nie, X. Chen, Biodegradable gold nanovesicles with an ultrastrong plasmonic coupling effect for photoacoustic imaging and photothermal therapy, Angew. Chemie - Int. Ed. (2013)https://doi.org/10.1002/anie.201308986.
[195] M. Hembury, C. Chiappini, S. Bertazzo, T.L. Kalber, G.L. Drisko, O. Ogunlade, S. Walker-Samuel, K.S. Krishna, C. Jumeaux, P. Beard, C.S.S.R. Kumar, A.E. Porter, M.F. Lythgoe, C. Boissière, C. Sanchez, M.M. Stevens, Gold–silica quantum rattles for multimodal imaging and therapy, Proc. Natl. Acad. Sci. (2015)https://doi.org/10.1073/pnas.1419622112.
[196] S.B. Lee, D. Kumar, Y. Li, I.K. Lee, S.J. Cho, S.K. Kim, S.W. Lee, S.Y. Jeong, J. Lee, Y.H. Jeon, PEGylated crushed gold shell-radiolabeled core nanoballs for in vivo tumor imaging with dual positron emission tomography and Cerenkov luminescent imaging, J. Nanobiotechnology. (2018)https://doi.org/10.1186/s12951-018-0366-x.
[197] J. Song, J. Zhou, H. Duan, Self-assembled plasmonic vesicles of SERS-encoded amphiphilic gold nanoparticles for cancer cell targeting and traceable intracellular drug delivery, J. Am. Chem. Soc. (2012)https://doi.org/10.1021/ja305154a.
[198] H. Deng, F. Dai, G. Ma, X. Zhang, Theranostic gold nanomicelles made from biocompatible comb-like polymers for thermochemotherapy and multifunctional imaging with rapid clearance, Adv. Mater. (2015)https://doi.org/10.1002/adma.201501420.
[199] P. Huang, P. Rong, J. Lin, W. Li, X. Yan, M.G. Zhang, L. Nie, G. Niu, J. Lu, W. Wang, X. Chen, Triphase interface synthesis of plasmonic gold bellflowers as near-infrared light mediated acoustic and thermal theranostics, J. Am. Chem. Soc. (2014) https://doi.org/10.1021/ja503115n.
[200] M.S. Mohamed, S. Veeranarayanan, A.C. Poulose, Y. Nagaoka, H. Minegishi, Y. Yoshida, T. Maekawa, D.S. Kumar, Type 1 ribotoxin-curcin conjugated biogenic gold nanoparticles for a multimodal therapeutic approach towards brain cancer, Biochim. Biophys. Acta (2014)https://doi.org/10.1016/j.bbagen.2013.12.020.
[201] J. Lin, S. Wang, P. Huang, Z. Wang, S. Chen, G. Niu, W. Li, J. He, D. Cui, G. Lu, X. Chen, Z. Nie, Photosensitizer-loaded gold vesicles with strong plasmonic coupling effect for imaging-guided photothermal/photodynamic therapy, ACS Nano. (2013) https://doi.org/10.1021/nn4011686.
[202] M. Zhou, R. Zhang, M. Huang, W. Lu, S. Song, M.P. Melancon, M. Tian, D. Liang, C. Li, A chelator-free multifunctional [^{64}Cu]CuS nanoparticle platform for simultaneous micro-PET/CT imaging and photothermal ablation therapy, J. Am. Chem. Soc. (2010)https://doi.org/10.1021/ja106855m.
[203] X.R. Song, X. Wang, S.X. Yu, J. Cao, S.H. Li, J. Li, G. Liu, H.H. Yang, X. Chen, Co_9Se_8 nanoplates as a new theranostic platform for photoacoustic/magnetic resonance dual-modal-imaging-guided chemo-photothermal combination therapy, Adv. Mater. (2015)https://doi.org/10.1002/adma.201405634.
[204] G. Ku, M. Zhou, S. Song, Q. Huang, J. Hazle, C. Li, Copper sulfide nanoparticles as a new class of photoacoustic contrast agent for deep tissue imaging at 1064 nm, ACS Nano. (2012)https://doi.org/10.1021/nn302782y.
[205] M. Zhou, J. Li, S. Liang, A.K. Sood, D. Liang, C. Li, CuS nanodots with ultrahigh efficient renal clearance for positron emission tomography imaging and image-guided photothermal therapy, ACS Nano. (2015)https://doi.org/10.1021/acsnano.5b02635.
[206] S. Zhang, C. Sun, J. Zeng, Q. Sun, G. Wang, Y. Wang, Y. Wu, S. Dou, M. Gao, Z. Li, Ambient aqueous synthesis of ultrasmall PEGylated $Cu_{2-x}Se$ nanoparticles as a multifunctional theranostic agent for multimodal imaging guided photothermal therapy of cancer, Adv. Mater. (2016)https://doi.org/10.1002/adma.201602193.
[207] L. Zhang, Z. Yang, W. Zhu, Z. Ye, Y. Yu, Z. Xu, J. Ren, P. Li, Dual-stimuli-responsive, polymer-microsphere-encapsulated CuS nanoparticles for magnetic resonance imaging guided synergistic chemo-photothermal therapy, ACS Biomater. Sci. Eng. (2017)https://doi.org/10.1021/acsbiomaterials.7b00204.
[208] Q. Feng, Y. Zhang, W. Zhang, Y. Hao, Y. Wang, H. Zhang, L. Hou, Z. Zhang, Programmed near-infrared light-responsive drug delivery system for combined magnetic tumor-targeting magnetic resonance imaging and chemo-phototherapy, Acta Biomater (2017)https://doi.org/10.1016/j.actbio.2016.11.035.
[209] G. Liang, X. Jin, H. Qin, D. Xing, Glutathione-capped, renal-clearable CuS nanodots for photoacoustic imaging and photothermal therapy, J. Mater. Chem. B. (2017) https://doi.org/10.1039/C7TB01517H.
[210] Q. Zhao, X. Yi, M. Li, X. Zhong, Q. Shi, K. Yang, High near-infrared absorbing Cu_5FeS_4 nanoparticles for dual-modal imaging and photothermal therapy, Nanoscale. (2016)https://doi.org/10.1039/C6NR04444A.
[211] S. Veeranarayanan, M.S. Mohamed, A.C. Poulose, M. Rinya, Y. Sakamoto, T. Maekawa, D.S. Kumar, Photodynamic therapy at ultra-low NIR laser power and X-Ray imaging using Cu_3BiS_3 nanocrystals, Theranostics (2018)https://doi.org/10.7150/thno.25286.
[212] Q. Wei, Y. Chen, X. Ma, J. Ji, Y. Qiao, B. Zhou, F. Ma, D. Ling, H. Zhang, M. Tian, J. Tian, M. Zhou, High-efficient clearable nanoparticles for multi-modal imaging and image-guided cancer therapy, Adv. Funct. Mater. (2018)https://doi.org/10.1002/adfm.201704634.
[213] A.C. Poulose, S. Veeranarayanan, M.S. Mohamed, Y. Nagaoka, R.R. Aburto, T. Mitcham, P.M. Ajayan, R.R. Bouchard, Y. Sakamoto, Y. Yoshida, T. Maekawa, D.S. Kumar, Multi-stimuli responsive Cu_2S nanocrystals as trimodal imaging and synergistic chemo-photothermal therapy agents, Nanoscale (2015)https://doi.org/10.1039/c4nr07139e.
[214] N. Lu, P. Huang, W. Fan, Z. Wang, Y. Liu, S. Wang, G. Zhang, J. Hu, W. Liu, G. Niu, R.D. Leapman, G. Lu, X. Chen, Tri-stimuli-responsive biodegradable theranostics for mild hyperthermia enhanced chemotherapy, Biomaterials (2017)https://doi.org/10.1016/j.biomaterials.2017.02.025.
[215] D. Gao, Z. Sheng, Y. Liu, D. Hu, J. Zhang, X. Zhang, H. Zheng, Z. Yuan, Protein-modified CuS nanotriangles: A potential multimodal nanoplatform for in vivo tumor photoacoustic/magnetic resonance dual-modal imaging, Adv. Healthc. Mater. (2017)https://doi.org/10.1002/adhm.201601094.
[216] A.C. Poulose, S. Veeranarayanan, M.S. Mohamed, R.R. Aburto, T. Mitcham, R.R. Bouchard, P.M. Ajayan, Y. Sakamoto, T. Maekawa, D.S. Kumar, Multifunctional $Cu_{2-x}Te$ nanocubes mediated combination therapy for multi-drug resistant MDA MB 453, Sci. Rep. 6 (2016), 35961.
[217] R. Chakravarty, S. Chakraborty, R.S. Ningthoujam, K.V.V. Nair, K.S. Sharma, A. Bailal, A. Guleria, A. Kunwari, H.D. Sarma, R.K. Vatsa, A. Dash, Industrial-scale synthesis of intrinsically radiolabeled ^{64}CuS nanoparticles for use in positron emission tomography (PET) imaging of cancer, Ind. Eng. Chem. Res. (2016)https://doi.org/10.1021/acs.iecr.6b03405.
[218] Q. Tian, F. Jiang, R. Zou, Q. Liu, Z. Chen, M. Zhu, S. Yang, J. Wang, J. Wang, J. Hu, Hydrophilic Cu_9S_5 nanocrystals: A photothermal agent with a 25.7% heat conversion efficiency for photothermal ablation of cancer cells in vivo, ACS Nano (2011) https://doi.org/10.1021/nn203293t.
[219] Q. Feng, W. Zhang, Y. Li, X. Yang, Y. Hao, H. Zhang, W. Li, L. Hou, Z. Zhang, An intelligent NIR-responsive chelate copper-based anticancer nanoplatform for synergistic tumor targeted chemo-phototherapy, Nanoscale. (2017)https://doi.org/10.1039/c7nr05003h.
[220] S. Zhang, H. Chen, G. Zhang, X. Kong, S. Yin, B. Li, L. Wu, An ultra-small thermosensitive nanocomposite with a Mo_{154}-core as a comprehensive platform for NIR-triggered photothermal-chemotherapy, J. Mater. Chem. B. (2018)https://doi.org/10.1039/c7tb02743e.
[221] L. Chen, Y. Feng, X. Zhou, Q. Zhang, W. Nie, W. Wang, Y. Zhang, C. He, One-pot synthesis of MoS_2 nanoflakes with desirable degradability for photothermal cancer therapy, ACS. Appl. Mater. Interfaces (2017)https://doi.org/10.1021/acsami.7b02657.
[222] S.S. Chou, B. Kaehr, J. Kim, B.M. Foley, M. De, P.E. Hopkins, J. Huang, C.J. Brinker, V.P. Dravid, Chemically exfoliated MoS_2 as near-infrared photothermal agents, Angew. Chemie - Int. Ed. (2013)https://doi.org/10.1002/anie.201209229.
[223] L. Chen, Y. Feng, X. Zhou, Q. Zhang, W. Nie, W. Wang, Y. Zhang, C. He, One-pot synthesis of MoS_2 nanoflakes with desirable degradability for photothermal cancer therapy, ACS Appl. Mater. Interfaces. (2017)https://doi.org/10.1021/acsami.7b02657.
[224] A.R. Hong, Y. Kim, T.S. Lee, S. Kim, K. Lee, G. Kim, H.S. Jang, Intense red-emitting upconversion nanophosphors (800 nm-Driven) with a core/double-shell structure for dual-modal upconversion luminescence and magnetic resonance in vivo imaging applications, ACS Appl. Mater. Interfaces. (2018)https://doi.org/10.1021/acsami.7b18078.
[225] J. Zuo, L. Tu, Q. Li, Y. Feng, I. Que, Y. Zhang, X. Liu, B. Xue, L.J. Cruz, Y. Chang, H. Zhang, X. Kong, Near infrared light sensitive ultraviolet-blue nanophotoswitch

for imaging-guided "off-On" therapy, ACS Nano. (2018)https://doi.org/10.1021/acsnano.7b07393.
[226] B. Zheng, H. Wang, H. Pan, C. Liang, W. Ji, L. Zhao, H. Chen, X. Gong, X. Wu, J. Chang, Near-infrared light triggered upconversion optogenetic nanosystem for cancer therapy, ACS Nano. (2017)https://doi.org/10.1021/acsnano.7b06395.
[227] L. Cheng, J. Liu, X. Gu, H. Gong, X. Shi, T. Liu, C. Wang, X. Wang, G. Liu, H. Xing, W. Bu, B. Sun, Z. Liu, PEGylated WS_2 nanosheets as a multifunctional theranostic agent for in vivo dual-modal CT/photoacoustic imaging guided photothermal therapy, Adv. Mater. (2014)https://doi.org/10.1002/adma.201304497.
[228] X. Qian, S. Shen, T. Liu, L. Cheng, Z. Liu, Two-dimensional TiS_2 nanosheets for in vivo photoacoustic imaging and photothermal cancer therapy, Nanoscale. (2015) https://doi.org/10.1039/C5NR00893J.
[229] L. Zhao, W. Yuan, H.P. Tham, H. Chen, P. Xing, H. Xiang, X. Yao, X. Qiu, Y. Dai, L. Zhu, F. Li, Y. Zhao, Fast-clearable nanocarriers conducting chemo/photothermal combination therapy to inhibit recurrence of malignant tumors, Small. (2017)https://doi.org/10.1002/smll.201700963.
[230] Z. Li, Y. Hu, M. Chang, K.A. Howard, X. Fan, Y. Sun, F. Besenbacher, M. Yu, Highly porous PEGylated Bi_2S_3 nano-urchins as a versatile platform for in vivo triple-modal imaging, photothermal therapy and drug delivery, Nanoscale. (2016)https://doi.org/10.1039/C6NR03398A.
[231] J. Liu, X. Zheng, L. Yan, L. Zhou, G. Tian, W. Yin, L. Wang, Y. Liu, Z. Hu, Z. Gu, C. Chen, Y. Zhao, Bismuth sulfide nanorods as a precision nanomedicine for in vivo multimodal imaging-guided photothermal therapy of tumor, ACS Nano. (2015)https://doi.org/10.1021/nn506137n.
[232] Y. Cui, J. Yang, Q. Zhou, P. Liang, Y. Wang, X. Gao, Y. Wang, Renal clearable Ag nanodots for in vivo computer tomography imaging and photothermal therapy, ACS Appl. Mater. Interfaces. (2017)https://doi.org/10.1021/acsami.6b16133.
[233] T. Yang, Y. Tang, L. Liu, X. Lv, Q. Wang, H. Ke, Y. Deng, H. Yang, X. Yang, G. Liu, Y. Zhao, H. Chen, Size-dependent Ag_2S nanodots for second near-infrared fluorescence/photoacoustics imaging and simultaneous photothermal therapy, ACS Nano. (2017)https://doi.org/10.1021/acsnano.6b07866.
[234] S. Wang, X. Li, Y. Chen, X. Cai, H. Yao, W. Gao, Y. Zheng, X. An, J. Shi, H. Chen, A facile one-pot synthesis of a two-dimensional MoS_2/Bi_2S_3 composite theranostic nanosystem for multi-modality tumor imaging and therapy, Adv. Mater. (2015) https://doi.org/10.1002/adma.201500870.
[235] R. Lv, P. Yang, F. He, S. Gai, C. Li, Y. Dai, G. Yang, J. Lin, A yolk-like multifunctional platform for multimodal imaging and synergistic therapy triggered by a single near-infrared light, ACS Nano. (2015)https://doi.org/10.1021/nn5063613.
[236] H. Moon, H. Kim, D. Kumar, H. Kim, C. Sim, J.H. Chang, J.M. Kim, D.K. Lim, Amplified photoacoustic performance and enhanced photothermal stability of reduced graphene oxide coated gold nanorods for sensitive photoacoustic imaging, ACS Nano. (2015)https://doi.org/10.1021/nn506516p.
[237] W. Dong, Y. Li, D. Niu, Z. Ma, J. Gu, Y. Chen, W. Zhao, X. Liu, C. Liu, J. Shi, Facile synthesis of monodisperse superparamagnetic Fe_3O_4 Core@hybrid@Au shell nanocomposite for bimodal imaging and photothermal therapy, Adv. Mater. (2011) https://doi.org/10.1002/adma.201103521.
[238] L. Cheng, C. Yuan, S. Shen, X. Yi, H. Gong, K. Yang, Z. Liu, Bottom-up synthesis of metal-ion-doped WS_2 nanoflakes for cancer theranostics, ACS Nano. (2015) https://doi.org/10.1021/acsnano.5b04606.
[239] Q. Tian, J. Hu, Y. Zhu, R. Zou, Z. Chen, S. Yang, R. Li, Q. Su, Y. Han, X. Liu, Sub-10 nm Fe_3O_4@$Cu_{2-x}S$ core−shell nanoparticles for dual-modal imaging and photothermal therapy, J. Am. Chem. Soc. (2013)https://doi.org/10.1021/ja4013497.
[240] Y. Il Park, H.M. Kim, J.H. Kim, K.C. Moon, B. Yoo, K.T. Lee, N. Lee, Y. Choi, W. Park, D. Ling, K. Na, W.K. Moon, S.H. Choi, H.S. Park, S.Y. Yoon, Y.D. Suh, S.H. Lee, T. Hyeon, Theranostic probe based on lanthanide-doped nanoparticles for simultaneous in vivo dual-modal imaging and photodynamic therapy, Adv. Mater. (2012) https://doi.org/10.1002/adma.201202433.
[241] X. Shi, H. Gong, Y. Li, C. Wang, L. Cheng, Z. Liu, Graphene-based magnetic plasmonic nanocomposite for dual bioimaging and photothermal therapy, Biomaterials. (2013)https://doi.org/10.1016/j.biomaterials.2013.03.023.
[242] X. Yi, K. Yang, C. Liang, X. Zhong, P. Ning, G. Song, D. Wang, C. Ge, C. Chen, Z. Chai, Z. Liu, Imaging-guided combined photothermal and radiotherapy to treat subcutaneous and metastatic tumors using iodine-131-doped copper sulfide nanoparticles, Adv. Funct. Mater. (2015)https://doi.org/10.1002/adfm.201502003.
[243] D.-W. Wang, X.-M. Zhu, S.-F. Lee, H.-M. Chan, H.-W. Li, S.K. Kong, J.C. Yu, C.H.K. Cheng, Y.-X.J. Wang, K.C.-F. Leung, Folate-conjugated Fe_3O_4@SiO_2@gold nanorods@mesoporous SiO_2 hybrid nanomaterial: a theranostic agent for magnetic resonance imaging and photothermal therapy, J. Mater. Chem. B. (2013)https://doi.org/10.1039/c3tb20090f.
[244] C. Li, T. Chen, I. Ocsoy, G. Zhu, E. Yasun, M. You, C. Wu, J. Zheng, E. Song, C.Z. Huang, W. Tan, Gold-coated Fe_3O_4 nanoroses with five unique functions for cancer cell targeting, imaging, and therapy, Adv. Funct. Mater. (2014)https://doi.org/10.1002/adfm.201301659.
[245] Y. Wang, H. Wang, D. Liu, S. Song, X. Wang, H. Zhang, Graphene oxide covalently grafted upconversion nanoparticles for combined NIR mediated imaging and photothermal/photodynamic cancer therapy, Biomaterials. (2013)https://doi.org/10.1016/j.biomaterials.2013.06.045.
[246] T. Liu, S. Shi, C. Liang, S. Shen, L. Cheng, C. Wang, X. Song, S. Goel, T.E. Barnhart, W. Cai, Z. Liu, Iron oxide decorated MoS_2 nanosheets with double PEGylation for chelator-free radiolabeling and multimodal imaging guided photothermal therapy, ACS Nano. (2015)https://doi.org/10.1021/nn506757x.
[247] R. Liu, L. Jing, D. Peng, Y. Li, J. Tian, Z. Dai, Manganese (II) chelate functionalized copper sulfide nanoparticles for efficient magnetic resonance/ photoacoustic dual-modal imaging guided photothermal therapy, Theranostics. (2015)https://doi.org/10.7150/thno.11754.
[248] K. Yang, L. Hu, X. Ma, S. Ye, L. Cheng, X. Shi, C. Li, Y. Li, Z. Liu, Multimodal imaging guided photothermal therapy using functionalized graphene nanosheets anchored with magnetic nanoparticles, Adv. Mater. (2012)https://doi.org/10.1002/adma.201104964.
[249] X. Wang, C. Wang, L. Cheng, S.-T. Lee, Z. Liu, Noble metal coated single-walled carbon nanotubes for applications in surface enhanced Raman scattering imaging and photothermal therapy, J. Am. Chem. Soc. (2012)https://doi.org/10.1021/ja300140c.
[250] Q. Feng, Y. Zhang, W. Zhang, Y. Hao, Y. Wang, H. Zhang, L. Hou, Z. Zhang, Programmed near-infrared light-responsive drug delivery system for combined magnetic tumor-targeting magnetic resonance imaging and chemo-phototherapy, Acta Biomater (2017)https://doi.org/10.1016/j.actbio.2016.11.035.
[251] M.S. Mohamed, A.C. Poulose, S. Veeranarayanan, R.R. Aburto, T. Mitcham, Y. Suzuki, Y. Sakamoto, P.M. Ajayan, R.R. Bouchard, Y. Yoshida, T. Maekawa, D.S. Kumar, Plasmonic fluorescent CdSe/Cu_2S hybrid nanocrystals for multichannel imaging and cancer directed photo-thermal therapy, Nanoscale (2016)https://doi.org/10.1039/c5nr05225d.
[252] S.H. Hu, Y.W. Chen, W.T. Hung, I.W. Chen, S.Y. Chen, Quantum-dot-tagged reduced graphene oxide nanocomposites for bright fluorescence bioimaging and photothermal therapy monitored in situ, Adv. Mater. (2012)https://doi.org/10.1002/adma.201104070.
[253] J. Huang, M. Guo, H. Ke, C. Zong, B. Ren, G. Liu, H. Shen, Y. Ma, X. Wang, H. Zhang, Z. Deng, H. Chen, Z. Zhang, Rational design and synthesis of γFe_2O_3@Au magnetic gold nanoflowers for efficient cancer theranostics, Adv. Mater. (2015)https://doi.org/10.1002/adma.201501942.
[254] Z.C. Wu, W.P. Li, C.H. Luo, C.H. Su, C.S. Yeh, Rattle-type Fe_3O_4@CuS developed to conduct magnetically guided photoinduced hyperthermia at first and second NIR biological windows, Adv. Funct. Mater. (2015)https://doi.org/10.1002/adfm.201503015.
[255] J. Song, X. Yang, O. Jacobson, L. Lin, P. Huang, G. Niu, Q. Ma, X. Chen, Sequential drug release and enhanced photothermal and photoacoustic effect of hybrid reduced graphene oxide-loaded ultrasmall gold nanorod vesicles for cancer therapy, ACS Nano. (2015)https://doi.org/10.1021/acsnano.5b03804.
[256] J. Yu, W. Yin, X. Zheng, G. Tian, X. Zhang, T. Bao, X. Dong, Z. Wang, Z. Gu, X. Ma, Y. Zhao, Smart MoS_2/Fe_3O_4 nanotheranostic for magnetically targeted photothermal therapy guided by magnetic resonance/photoacoustic imaging, Theranostics. (2015)https://doi.org/10.7150/thno.11802.
[257] G. Yang, H. Gong, T. Liu, X. Sun, L. Cheng, Z. Liu, Two-dimensional magnetic WS_2@Fe_3O_4 nanocomposite with mesoporous silica coating for drug delivery and imaging-guided therapy of cancer, Biomaterials. (2015)https://doi.org/10.1016/j.biomaterials.2015.04.053.
[258] J. Li, Z. Lyv, Y. Li, H. Liu, J. Wang, W. Zhan, H. Chen, H. Chen, X. Li, A theranostic prodrug delivery system based on Pt(IV) conjugated nano-graphene oxide with synergistic effect to enhance the therapeutic efficacy of Pt drug, Biomaterials. (2015)https://doi.org/10.1016/j.biomaterials.2015.01.074.
[259] X. Wang, D. Cao, X. Tang, J. Yang, D. Jiang, M. Liu, N. He, Z. Wang, Coating Carbon Nanosphere with Patchy Gold for Production of Highly Efficient Photothermal Agent, ACS Appl. Mater. Interfaces. (2016)https://doi.org/10.1021/acsami.6b05550.
[260] D.Y. Santiesteban, D.S. Dumani, D. Profili, S.Y. Emelianov, Copper Sulfide Perfluorocarbon Nanodroplets as Clinically Relevant Photoacoustic/Ultrasound Imaging Agents, Nano Lett. (2017)https://doi.org/10.1021/acs.nanolett.7b02105.
[261] M. Chen, S. Tang, Z. Guo, X. Wang, S. Mo, X. Huang, G. Liu, N. Zheng, Core-shell Pd@Au nanoplates as theranostic agents for in-vivo photoacoustic imaging, CT imaging, and photothermal therapy, Adv. Mater. (2014)https://doi.org/10.1002/adma.201404013.
[262] A.Y. Lin, J.K. Young, A.V. Nixon, R.A. Drezek, Encapsulated Fe_3O_4/Ag complexed cores in hollow gold nanoshells for enhanced theranostic magnetic resonance imaging and photothermal therapy, Small. (2014)https://doi.org/10.1002/smll.201303593.
[263] E. Li, X. Cheng, Y. Deng, J. Zhu, X. Xu, P.E. Saw, H. Gu, C. Ge, Y. Pan, Fabrication of PEGylated Fe@Bi_2S_3 nanocomposites for dual-mode imaging and synergistic thermoradiotherapy, Biomater. Sci. (2018)https://doi.org/10.1039/C8BM00336J.
[264] K. Yang, G. Yang, L. Chen, L. Cheng, L. Wang, C. Ge, Z. Liu, FeS nanoplates as a multifunctional nano-theranostic for magnetic resonance imaging guided photothermal therapy, Biomaterials. (2015)https://doi.org/10.1016/j.biomaterials.2014.10.052.
[265] Y. Dai, H. Xiao, J. Liu, Q. Yuan, P. Ma, D. Yang, C. Li, Z. Cheng, Z. Hou, P. Yang, J. Lin, In vivo multimodality imaging and cancer therapy by near-infrared light-triggered trans -platinum pro-drug-conjugated upconverison nanoparticles, J. Am. Chem. Soc. (2013)https://doi.org/10.1021/ja410028q.
[266] L. Dong, G. Ji, Y. Liu, X. Xu, P. Lei, K. Du, S. Song, J. Feng, H. Zhang, Multifunctional Cu-Ag_2S nanoparticles with high photothermal conversion efficiency for photoacoustic imaging-guided photothermal therapy in vivo, Nanoscale (2018)https://doi.org/10.1039/C7NR07263E.
[267] G. Lv, W. Guo, W. Zhang, T. Zhang, S. Li, S. Chen, A.S. Eltahan, D. Wang, Y. Wang, J. Zhang, P.C. Wang, J. Chang, X.J. Liang, Near-Infrared Emission CuInS/ZnS Quantum Dots: All-in-One Theranostic Nanomedicines with Intrinsic Fluorescence/Photoacoustic Imaging for Tumor Phototherapy, ACS Nano. (2016)https://doi.org/10.1021/acsnano.6b05419.
[268] F. Wang, Q. Sun, B. Feng, Z. Xu, J. Zhang, J. Xu, L. Lu, H. Yu, M. Wang, Y. Li, W. Zhang, Polydopamine-Functionalized Graphene Oxide Loaded with Gold Nanostars and Doxorubicin for Combined Photothermal and Chemotherapy of Metastatic Breast Cancer, Adv. Healthc. Mater. (2016)https://doi.org/10.1002/adhm.201600283.
[269] P. Bouziotis, D. Stellas, E. Thomas, C. Truillet, C. Tsoukalas, F. Lux, T. Tsotakos, S. Xanthopoulos, M. Paravatou-Petsotas, A. Gaitanis, L.A. Moulopoulos, V.

Koutoulidis, C.D. Anagnostopoulos, O. Tillement, ^{68}Ga-radiolabeled AGuIX nanoparticles as dual-modality imaging agents for PET/MRI-guided radiation therapy, Nanomedicine. (2017)https://doi.org/10.2217/nnm-2017-0032.
[270] B. Jang, J.Y. Park, C.H. Tung, I.H. Kim, Y. Choi, Gold nanorod-photosensitizer complex for near-infrared fluorescence imaging and photodynamic/photothermal therapy in vivo, ACS Nano. (2011)https://doi.org/10.1021/nn102722z.
[271] J. Yao, J. Feng, J. Chen, External-stimuli responsive systems for cancer theranostic, Asian J. Pharm. Sci. (2016)https://doi.org/10.1016/j.ajps.2016.06.001.
[272] L. Zhou, H. Wang, Y. Li, Stimuli-responsive nanomadicines for overcoming cancer multidrug resistance, Theranostics (2018)https://doi.org/10.7150/thno.22679.
[273] NCT00978562DSC-MRI With Ferumoxytol and DCE-MRI With Gadolinium in Imaging Vascular Properties in Younger Patients With Brain Tumors
[274] NCT00103038: Ferumoxytol in Improving MR Imaging in Patients With High-Grade Brain Tumors or Cerebral Metastases.
[275] NCT01663090: Ferumoxytol-Enhanced MRI in Adult/Pedi Sarcomas.
[276] NCT03234309: Ferumoxytol in Magnetic Resonance Imaging of Pediatric Patients With Brain Tumors.
[277] NCT03179449: In Vivo Characterization of Macrophages in Pediatric Patients With Malignant Brain Tumors Using Ferumoxytol-enhanced MRI.
[278] NCT02857218: Ferumoxytol-Enhanced MRI in Imaging Lymph Nodes in Patients With Stage IIB-IIIC Esophageal Cancer.
[279] NCT03325166: Pembrolizumab and Magnetic Resonance Imaging With Ferumoxytol in Treating Patients With Non-small Cell Lung Cancer and Brain Metastases.
[280] NCT01336803: Differentiation of Bone Sarcomas and Osteomyelitis With Ferumoxytol-Enhanced MRI.
[281] NCT03280277: Ferumoxytol-Enhanced MRI in Imaging Lymph Nodes in Patients With Locally Advanced Rectal Cancer.
[282] NCT01770353: MM-398 (Nanoliposomal Irinotecan, Nal-IRI) to Determine Tumor Drug Levels and to Evaluate the Feasibility of Ferumoxytol Magnetic Resonance Imaging to Measure Tumor Associated Macrophages and to Predict Patient Response to Treatment.
[283] NCT00659126: Ferumoxytol- and Gadolinium-Labeled MRI in Measuring Tumors Before or After Treatment in Patients With Primary or Metastatic Brain Tumors.
[284] NCT02689401: MRI Iron Oxide Imaging for Lymph Node Staging in Esophageal Cancer.
[285] NCT01895829: Ferumoxytol - Iron Oxide Nanoparticle Magnetic Resonance Dynamic Contrast Enhanced MRI.
[286] NCT01815333: Clinical and Technical Feasibility of a Ultrasuperparamagnetic Nanoparticle Iron Oxide (USPIO)-Enhanced Magnetic Resonance Lymph Node Imaging.
[287] NCT02141490: Study of Ferumoxytol Enhanced MRI for Detecting Lymph Node Metastases in Prostate, Bladder, and Kidney Cancers.
[288] NCT01927887: Pre-Operative Nodal Staging of Thyroid Cancer Using USPIO MRI: Preliminary Study.
[289] NCT02253602: Innovative MRI Techniques to Improve Treatment Stratification of Patients With Esophageal Cancer (IMPROVE)
[290] NCT01542879: Pilot Development of Radiation Free Whole Body Magnetic Resonance (MR) Imaging Technique for Staging Children With Cancer.
[291] NCT02359097: Steady State Blood Volume Maps Using Ferumoxytol Non-stoichiometric Magnetite MRI in Imaging Patients With Glioblastoma.
[292] NCT00660543: MRI Study With Ferumoxytol in Assessing Early Response in Patients With Glioblastoma Multiforme Receiving Temozolomide and Radiation Therapy.
[293] NCT00087347: Magnetic Resonance Imaging of Lymph Nodes Using Ferumoxytol in Patients With Primary Prostate or Breast Cancer.
[294] NCT03347617: Ferumoxytol MRI in Assessing Response to Pembrolizumab in Patients With Brain Tumors From Melanoma and Glioblastoma.
[295] NCT01296139: Ferumoxytol Enhanced MRI for the Detection of Lymph Node Involvement in Prostate Cancer.
[296] NCT01983371: Diagnostic Accuracy of Ferumoxytol-Enhanced MRI for Detecting Lymph Node Metastases in Colorectal Cancer.
[297] NCT00769093: Assessing Dynamic Magnetic Resonance (MR) Imaging in Patients With Recurrent High Grade Glioma Receiving Chemotherapy.
[298] NCT02466828: qBOLD MRI of Glioblastoma Multiforme for Assessment of Tumor Hypoxia.
[299] NCT00416455: Fludeoxyglucose F 18 PET Scan: , CT Scan, and Ferumoxtran-10 MRI Scan Before Chemotherapy and Radiation Therapy in Finding Lymph Node Metastasis in Patients With Locally Advanced Cervical Cancer or High-Risk Endometrial Cancer.
[300] NCT00147238: A Validation Study of MR Lymphangiography Using SPIO, a New Lymphotropic Superparamagnetic Nanoparticle Contrast.
[301] NCT02751606: Nano MRI on 7 Tesla in Rectal and Breast Cancer.
[302] NCT03223064: Accuracy of Lymph Node Imaging in Prostate Cancer: PSMA PET-CT and Nano-MRI (MAGNIFY).
[303] NCT00107484: Magnetic Resonance Imaging Using Ferumoxtran-10 in Finding Metastases to the Axillary Lymph Nodes in Patients With Breast Cancer.
[304] NCT00659334: Imaging of Intravenous (IV) Combidex to Brain, Intra-cerebral Tumors and in Central Nervous System (CNS) Inflammation.
[305] NCT00188695: Combidex USPIO - Ultra-Small Superparamagnetic Iron Oxide.
[306] NCT00920023: Pre-Operative Staging of Pancreatic Cancer Using Superparamagnetic Iron Oxide Magnetic Resonance Imaging (SPIO MRI).
[307] NCT00436410: Tumor Necrosis Factor in Patients Undergoing Surgery for Primary Cancer or Metastatic Cancer.
[308] NCT02106598: Targeted Silica Nanoparticles for Real-Time Image-Guided Intraoperative Mapping of Nodal Metastases.
[309] NCT01790399: Identification of Sentinel Node(s) in Breast Cancer (SENTIMAG)
[310] NCT02249208: Sentinel Lymph Node Biopsy With Superparamagnetic Iron Oxide for Breast Cancer Patients After Neoadjuvant Treatment. (SENTINAC-01).
[311] NCT02465593: A Study of PEP503(Radio-enhancer) With Radiotherapy and Chemotherapy for Patients With Rectal Cancer.
[312] NCT02805894: NBTXR3 Nanoparticles and EBRT or EBRT With Brachytherapy in the Treatment of Prostate Adenocarcinoma.